The influence of shelf bathymetry and beach topography on extreme total water levels: Linking large-scale changes of the wave climate to local coastal hazards

Katherine A. Serafin[a,d,*], Peter Ruggiero[a], Patrick L. Barnard[b], Hilary F. Stockdon[c]

[a] *College of Earth, Ocean, and Atmospheric Sciences, Oregon State University, Corvallis, OR, USA*
[b] *Pacific Coastal and Marine Science Center, U.S. Geological Survey, Santa Cruz, CA, USA*
[c] *St. Petersburg Coastal and Marine Science Center, U.S. Geological Survey, St. Petersburg, FL, USA*
[d] *Present Address: Department of Geophysics, Stanford University, Stanford, CA, USA*

Abstract

Total water levels (TWLs) at the coast are driven by a combination of deterministic (e.g., tides) and stochastic (e.g., waves, storm surge, and sea level anomalies) processes. The contribution of each process to TWLs varies depending on regional differences in climate and framework geology, as well as local-scale variations in beach morphology, coastal orientation, and shelf bathymetry. Large-scale changes to the climate altering the frequency, direction, and intensity of storms, may therefore propagate to the nearshore differently, amplifying or suppressing local coastal hazards and changing the exposure of coastal communities to extreme TWLs. This study investigates the hydrodynamic and geomorphologic factors controlling local TWLs along high-energy United States coastlines where wave-influences dominate TWLs. Three study sites in the states of Washington, Oregon, and California are chosen to explore how regional and local differences in beach topography and wave transformation over shelf bathymetry drives variations in the magnitude and impacts of extreme TWLs. Results indicate that TWLs are most influenced by wave transformation processes in locations with steep beach slopes and complex offshore bathymetry, while beach topography influences the severity of coastal impacts. Once the relative morphologic controls on TWLs are better understood, hypothetical future climate scenarios are explored to assess how changes to the average deepwater wave climate (height, period, and direction) may alter local TWLs when compared to estimates of likely sea level rise and future coastal management strategies. Changes to the wave climate are found to be as detrimental to the coastline as sea level rise in some locations, where small variations of the TWL drive large, nonlinear changes in hours of impact to the backshore beach. Overall, this study develops an approach for quantifying the range of hydrodynamic and morphologic controls on the magnitude of TWLs which will ultimately better prepare coastal communities for uncertain changes to the global climate.

Keywords: total water levels, wave climate, runup, morphology, bathymetry, climate change, US West coast

---

1. Introduction

Sea level variability at the coast is driven by numerous processes varying over timescales of hours to days (e.g., storm surge and tides [1]), months to years (e.g., seasonal cycles, ocean/atmospheric variability, eddies, and gyres [2, 3, 4, 5]), and decades to centuries (e.g., vertical land motion, thermal expansion, and ice melt [6, 7]). Global sea level has risen 1.7 mm/yr over the last century [8] and 3.4 mm/yr since the early 1990s [9]. Recent observations suggest this rate has accelerated over the last 25 years [10]. Paired with intra- and interannual sea level variability, rising seas will continue to impact coastal communities with more frequent flooding [11, 12].

On open coast beaches, the wave-induced water level, or wave runup, the combination of wave setup and swash processes [13, 14, 15, 16], acts on top of sea levels, extending the reach of high water levels farther inland to drive flooding and erosion. While understanding the mechanisms driving wave runup has been an active area of research over the last few decades (e.g., [17, 18, 19, 20, 21, 22, 23, 13, 24, 14, 15]), there has been less focus on how changes to the wave climate will affect total water levels at the shoreline. Without an understanding of how future changes to storminess may impact the coast, coastal communities will lack crucial information to adequately plan for future hazards.

*Corresponding author
Email address: kserafin@stanford.edu (Katherine A. Serafin)

Wave runup, dependent on both the wave climate and local beach characteristics [23, 25, 14], is a major contributor to coastal total water levels (TWL; [26, 27, 28]) and flooding and erosion events [29, 30, 31]. The understanding of the contribution of waves to extreme TWLs, however, has thus far been presented on a global [26] or regional basis [27, 28], limiting analyses to the large-scale hydrodynamic and climatic processes driving TWLs, rather than local-scale influences. Much like the temporal and spatial variations in hydrodynamic processes driving variability in coastal sea levels, spatial and temporal variations in local beach morphology and wave conditions can lead to corresponding variability in both setup and swash.

Wave runup is often parameterized as a function of wave height, wave length (which is a function of wave period), and local beach slope [23, 25, 14]. The slope of the beach topography is typically measured around the shoreline, termed foreshore beach slope, or from the shoreline to the dune toe, termed backshore beach slope. Beach slopes vary spatially and temporally due to wave climate, grain-size, and sediment supply [32]. Seasonal and storm-induced changes in beach slope can therefore lead to differences on the order of 1 m in wave runup [33]. A number of studies have also suggested that the nearshore morphology, in particular the presence, shape, and variability of sandbars, may influence swash processes [34, 35]. However, Cohn and Ruggiero [19] tested the relative influence of nearshore morphology and beach slope on wave runup using a numerical model and found beach slope to have a stronger influence on the elevation of wave runup than variability in subaqueous sandbars.

Local variations in wave-induced water levels are also driven by differences in shelf morphology. Deep-water waves are subject to changes in their height, period, and direction, as they propagate over shelf bathymetry towards the shore. Morphologic features such as canyons, banks, capes, headlands, and islands may focus, divert, and/or transform wave energy through refraction, shoaling, diffraction, and dissipation [36, 37]. Waves measured at offshore buoys in deep water may therefore be very different than those that have traveled across the shelf [38], potentially producing longshore variation in TWLs.

Despite the importance of the above-mentioned wave transformation processes in driving nearshore variation in the wave climate, global [39, 40] and regional [41, 42, 43, 44] projections of the future wave climate have thus far focused on changes to deep-water conditions. Across the Northern hemisphere, the average wave height is projected to decrease, while in contrast, there may be significant wave height increases in the tropics and Southern hemisphere [39, 40]. Furthermore, future changes to the global climate may increase the frequency of strong El Niño events [45], which alters the frequency, intensity, and track of storms across the Northeast Pacific. Thus, a changing climate will drive regional variation in the magnitude and frequency of storms.

Along the mainland West coast of the United States (US), mean wave height is projected to decrease by approximately 2 to 20% [39, 42, 40], mean wave period is projected to increase by approximately 2 to 5% [42, 40], and mean wave direction is projected to shift anticlockwise (more waves from the south) by approximately 2 to 5% by 2100 [42, 40]. While significant progress has been made in projecting future deep-water wave conditions, downscaling of the deep-water wave conditions to the nearshore must be completed on a site to site basis to understand the local affects of these changes, which is computationally demanding and time intensive.

In specific locations (e.g., the Hawaiian islands [46], coastlines in northern and southern California [47, 48]), as well as more generally on beaches, harbors, or structures [49], studies have begun to investigate the local consequences of future changes to the wave climate. Barnard et al. [48] and Erikson et al. [47] used future wave projections from dynamically downscaled Global Climate Models (GCMs) [42] to estimate flooding through an event-based approach by pairing low-probability storm events with sea level rise scenarios. Shope et al. [46] modeled the mean of the top 5% of winter and summer wave heights, as well as a range of incremental increases to this average based on potential changes in extreme dynamically downscaled wave conditions by 2100 [50]. Sierra and Casas-Prat [49] used another approach, exploring the range of variability to the future wave climate documented in the broader literature. Findings across all studies indicate modifications to wave forcings can have a measurable effect on physical processes such as erosion, overtopping, or flooding affecting coastal regions. Our study uses similar methodologies to Sierra and Casas-Prat [49] by investigating hypothetical future shifts in the wave climate, allowing for the analysis of many future outcomes without the limitations of computational demands from downscaling many GCMs. Hypothetical distribution shifts can also be used to explore the existence of "tipping points" (i.e., how small changes to the system may drive large, significant changes) under various changes to climatic variables.

Changes to the wave climate and sea level alone are not the only drivers of coastal change, as more uncertainty lies in changes to future morphological evolution, which rarely is considered in risk assessments of future coastlines. Recent research has shown that human modifications can alter coastlines just as much as changes to the future climate, and in some cases, make communities more prone to flooding due to specific adaptation interventions [51, 52, 53]. For example, coastal armoring (e.g., sea walls, rip rap revetments, etc.) is one form of protection used to prevent flooding and dune or bluff erosion. Hard armoring often cuts off the sediment supply to the beach, generating local erosion and steepening beach slopes. This steepening can drive a positive feedback loop, where steeper profiles cause higher TWLs, which in turn erode the beach face, continuing profile steepening. Beach nourishment often has the opposite effect (as long as the nourishment project lasts or is renourished) and flattens the beach.

Because changes to the climate will alter storm systems in different manners around the world, this study develops an approach to quantify the many factors that control local coastal hazards (e.g., wave climate, beach morphology, and sea level) by comparing three sandy beaches on the high-energy, US West coast (one each in Washington, Oregon, and California). First, the influence of wave transformation over shelf bathymetry on coastal TWLs is investigated, then we explore the role that the spatial and temporal variability of beach topography plays in altering the magnitude of TWLs. Finally, hypothetical distribution shifts to the average wave height, wave period, mean wave direction, sea level, and beach slope are used to evaluate how future changes to each variable may affect the elevation of TWLs and their related impacts at each study site. Disentangling the relative morphological controls on TWLs will help to better understand the dominant drivers of local-scale coastal impacts like flooding and erosion, which are relevant to planning and adaptation.

2. Datasets and Methods

Three distinct sites along the high-energy US West coast (Figure 1) with near-complete wave and water level records, similar shelf widths, and high-resolution spatial and temporal beach topography were chosen to examine how regional differences in shelf bathymetry and beach topography influence extreme TWLs. Locations were selected due to the availability of high-resolution topographic data [54, 55, 56], previously known gradients in wave heights along nearshore contours due to wave transformation processes [36, 57], and the importance of the contribution of wave runup to extreme TWLs at each site [27].

Our analysis is divided into four parts. First, we develop TWL time series at each site using deep-water waves and a uniform beach slope, representative of regional-scale morphology and hydrodynamic forcings. Next, we evaluate the influence of shelf bathymetry and beach topography on wave runup by producing multiple alongshore-varying TWL time series at each site, using 1) nearshore-transformed waves and a uniform beach slope, 2) nearshore-transformed waves and spatially-varying beach slopes, and 3) nearshore-transformed waves and temporally-varying beach slopes. The spatially-varying TWLs compared to the regional TWLs provide insight into the relative control each variable has on coastal TWLs, as well as the consequences for not including local features in TWL computations. Once the controls of morphology on TWLs have been fully assessed, we approximate how often extreme and hourly TWLs reach backshore beach features to better understand how spatial variations in TWL magnitude may affect the shoreline. Finally, we simulate hypothetical future climate conditions by shifting the average distribution of each wave climate variable (e.g., wave height, period, and direction) by a predefined amount and re-compute TWLs to estimate how a change to wave conditions may precipitate site-specific coastal hazards.

2.1. Study Sites

The North Beach subcell is a prograding, 30 km stretch of coastline in Grays Harbor County, Washington and is the most northern subcell of the greater Columbia River Littoral Cell. The Columbia River Littoral Cell is characterized by wide, gently-sloping, dissipative beaches, the majority of which are backed by prograding dune fields [58]. On average, the

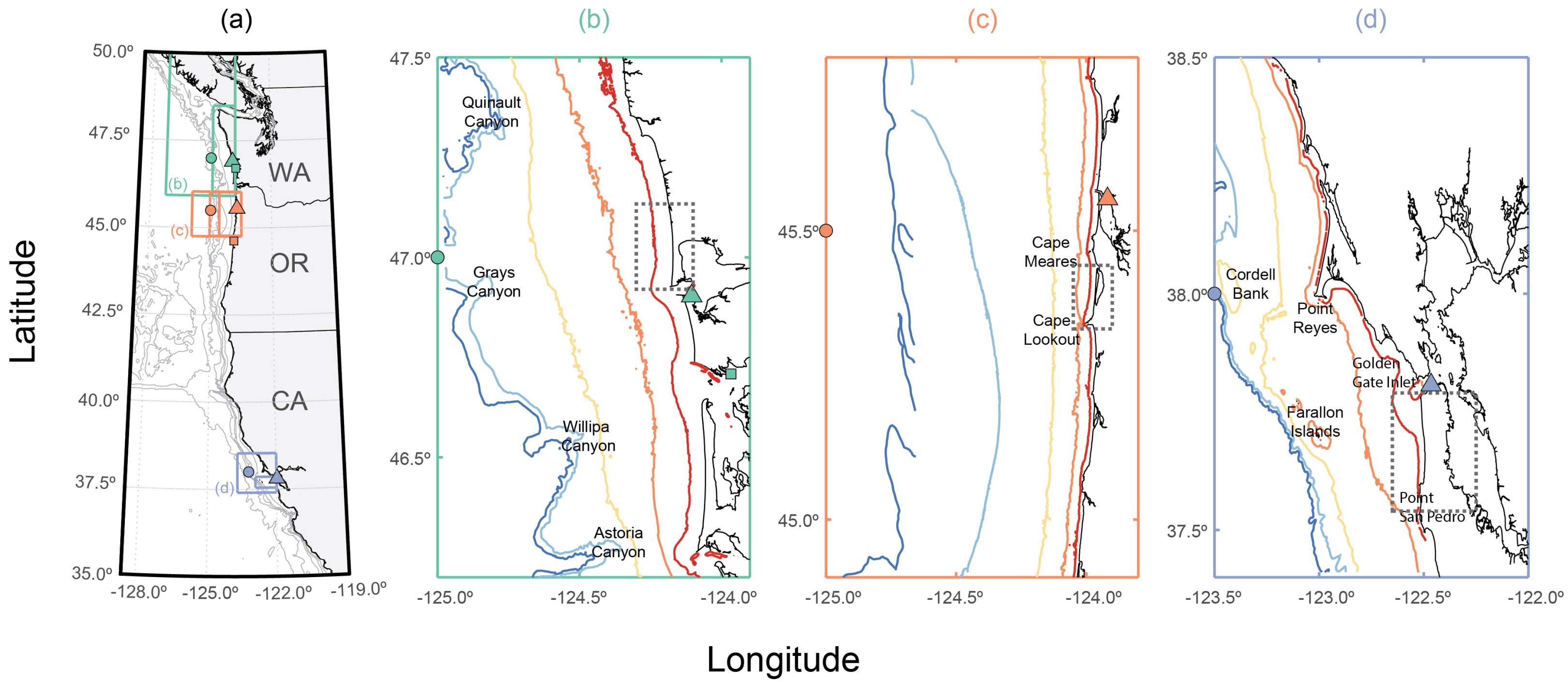

Figure 1: Map of regional (a) and specific study site (b-d) locations. The regional map (a) includes SWAN modeling domains for nearshore wave transformations, where the outer SWAN grids are relatively coarse and higher resolution grids are nested within. Bathymetry contours (in grey) are at 100, 250, 500, 1000, and 3000 m depths. The site specific maps depict the shelf bathymetry offshore of the (b) North Beach subcell (WA), (c) Netarts Littoral Cell (OR), and (d) San Francisco Littoral Cell (CA). Gray, dashed-line boxes represent the extent of each specific study site. Contours for all locations are depicted at the shoreline (black), 20 (red), 50 (orange), 100 (yellow), 250 (light blue), and 500 (dark blue) m depths. Across all maps, circles represent the shelf-edge wave hindcast nodes, triangles represent the primary tide gauges, and squares represent the secondary tide gauges, where green, orange, and blue colors represent the WA, OR, and CA study sites, respectively.

mean grain size is 0.16 mm, containing some of the finest grain size and lowest sloping beaches within the Columbia River Littoral Cell [59, 58]. Offshore, the continental shelf is fairly narrow (30-40 km to the shelf edge) and contains many pronounced canyons (Figure 1b). Grays Canyon lies directly offshore of the North Beach subcell, and is bounded by Quinault Canyon to the north and Willapa Canyon to the south. Annual average deep-water wave height, period, and direction is 2.5 m, 11 s, and 270° (arriving from the west), respectively. During the winter, the average deep-water wave height, period and direction is 3 m, 12 s, and 260° (arriving from slightly south of west). Tides are meso-tidal, with a mean range of 2.13 m [60].

The Netarts Littoral Cell is a 17 km pocket beach on the northern Oregon coastline in Tillamook County. The Netarts Littoral Cell is bounded by two erosion resistant headlands, Cape Lookout to the south and Cape Meares to the north. The headlands extend to deep water, restricting sediment transport between them. In general, the steepest beach slopes are adjacent to the headlands, where the beach is composed of sediment locally sourced from the headlands [61]. The mean grain size for the cell is 0.17 mm, classified as fine sand [59]. The Oregon continental shelf is also fairly narrow (15-20 km to the shelf edge) and uniform (Figure 1c), but contains banks to the south and the Astoria Canyon to the north (shown in Figure 1b). This study focuses on Netarts spit, a 9 km stretch of coastline in the Netarts Littoral Cell home to Cape Lookout State Park, a popular campsite and day use area on the Oregon coast. The erosion on Netarts Spit was minimal prior to the 1982/83 El Niño [62]. However, post 1982/82 El Niño, the Netarts Spit has been eroding along the southern end of the cell and accreting towards the north [63, 62]. The annual average deep-water wave height, peak period, and direction in the region is 2.5 m, 11 s, and 275° (arriving from slightly north of west) and 3 m, 12 s, and 265° (arriving from slightly south of west) during the winter, similar to the Washington wave climate. Tides are micro-tidal, with a mean range of 1.90 m [60].

The San Francisco Littoral Cell extends from Point Reyes to Point San Pedro and is located in north-central California. Our study site focuses specifically on an approximately 25 km stretch of coastline extending from Golden Gate inlet southward to Point San Pedro

(Figure 1d). This stretch of coastline consists of sandy beaches, sea cliffs and bluffs, and a continental shelf extending 40-50 km to the shelf edge. Large parts of the coast are highly urbanized with rip-rap and seawalls to protect vulnerable coastal communities and critical infrastructure. The northern extent of our study site, Ocean Beach, is located directly south of the Golden Gate inlet and is impacted by a massive ebb tidal delta [57] that covers a surface area of 150 km^2 and has significantly evolved over the last century due to changes in sediment supply [64]. The southern extent of Ocean Beach has experienced decadal-scale trends in erosion [64, 56, 65], while the northern extent has been accreting [66, 55].

The mean grain size for Ocean Beach is 0.3 mm [56], classified as medium sand, and coarser than the Washington and Oregon study sites. While the San Francisco Littoral Cell is north-south trending, the California shoreline is oriented slightly more south than the Oregon and Washington study sites, whose shoreline's are west-facing. Complex offshore bathymetry includes Cordell Bank off Point Reyes to the north, a small canyon to the south, the Farallon Islands directly offshore, and in the nearshore, the Golden Gate ebb-tidal delta. The northern California coastline is subject to slightly smaller, but longer period, waves than Washington and Oregon, coming from predominantly the northwest. The annual average deep-water wave height, peak period, and direction in the region is 2.5 m, 12 s, and 290° (arriving from the west northwest) and 2.7 m, 13 s, and 280° (arriving from the west northwest) during the winter. Tides are micro-tidal, with a mean range of 1.25 m [60].

Hereinafter, each study site is identified by their state acronym, where WA, OR, and CA, refer to the North Beach subcell, the Netarts Littoral Cell, and the San Francisco Littoral Cell, respectively.

2.2. Developing Regional Total Water Level Time Series

Total water levels were computed at each study site by linearly superimposing measured still water levels (SWL) extracted from tide gauges, with wave runup (R), such that

$$TWL = SWL + R. \tag{1}$$

Many empirical formulations parameterize the $R_{2\%}$, the 2% exceedance percentile of runup maxima, as a function of deep-water significant wave height (Hs), wave period (T) or wave length (L_0), and beach slope (β) (e.g., [18, 25, 23]). Here we employ the Stockdon et al. [23] empirical model,

$$R_{2\%} = 1.1\left(0.35\beta\left(H_sL_0\right)^{\frac{1}{2}} + \frac{\left[H_sL_0\left(0.563\beta^2 + 0.004\right)\right]^{\frac{1}{2}}}{2}\right) \tag{2}$$

developed using data from 10 field experiments across 6 beaches, including data from the US West coast.

Hourly measured SWLs were extracted from National Oceanic and Atmospheric Administration (NOAA) operated tide gauges nearest to each study site (Figure 1). The closest tide gauge record to the study site did not always have an acceptable record length for producing statistics on extreme events, so records with less than 15 years of data were merged with a secondary tide gauge, chosen as the nearest tide gauge to the primary tide gauge with a longer, more complete record length (see Appendix A for detailed merging methodologies). Each combined SWL record was then paired with a shelf-edge wave climate (i.e., wave height, period, and direction) extracted from the Global Ocean Waves 2 (GOW2) wave hindcast database [67].

Wave hindcasts were used due to their consistent record length and shelf-edge spatial resolution of one quarter degree. The GOW2 reanalysis datasets provide hourly time series of Hs, wave peak frequency (transformed into peak period, Tp), and mean wave direction (MWD) from 1979 through 2015. Validation with both altimeter and buoy observations show GOW2 preforms well along the US West coast, with a high Pearson correlation coefficient, less than 10 cm of bias, and a RMSE less than 20 cm for the mean wave climate [67]. Due to the hourly resolution wind forcing used in the numerical modeling, extreme wave heights are also well represented. The 99.5th percentile of wave height is slightly negatively biased (less than 20 cm) along the US West coast when compared to observational records [67].

Beach slopes were extracted every 5-10 m [68] from a 2002 NASA/USGS lidar survey (for Washington and Oregon [69]) and at a slightly coarser resolution [65] from a 1998 NOAA/NASA/USGS lidar survey (for California [70]; see Appendix B for beach slope extraction methodologies). A regionally-uniform beach slope (β_R) was determined by averaging beach slopes extracted from the lidar data at each location and resulted in an average (standard deviation) β_R of 0.02 (0.009), 0.05 (0.019), and 0.07 (0.025), in WA, OR, and CA, respectively. Once SWLs and $R_{2\%}$ time series for each study site were finalized, TWLs were calculated using Eqn 1. The final TWL_R records are hourly and over 96% complete for the 35 year period 1980 to 2015 for each location (Table 1).

2.3. Developing Local Total Water Level Time Series

In order to understand the influence of shelf bathymetry on the magnitude of TWLs at each study site, offshore wave conditions were transformed to the nearshore and extracted every 500 m. $R_2\%$ was computed using β_R coupled with alongshore-varying, nearshore waves and then added to the regional SWLs.

Previously developed lookup tables (see Allan et al. [61] and Eshleman et al. [57] for detailed methods) were used to dynamically transform offshore, deep-water wave triplets (Hs, Tp, MWD) to their alongshore-varying, nearshore equivalents in an efficient manner. To develop each study site's lookup tables, the wave climate was discretized into 2,000 to 4,000 wave conditions which represented many possible ranges of joint-conditions at each site. These representative wave conditions were then simulated using stationary model runs of SWAN [71] over a course outer grid and one to two nested grids with resolutions ranging from 2000 m (outer grid in both directions) to 100 m (inner grid in both directions). See Figure 1a for SWAN modeling domains and Table 2 for generalized model specifications at each location.

The lookup tables were then used to interpolate nearshore wave conditions (here defined at the 20 m contour or where waves first break due to depth constraints, i.e., depth limited breaking, $\gamma = 0.42$) from the shelf-edge GOW2 wave conditions. This methodology allows for the simple extraction of nearshore wave conditions without running SWAN for every hourly wave event over the 35 year long record at each study site. Waves were extracted at the resolution of the finest SWAN grid (200, 100, and 200 m for WA, OR, and CA, respectively). Nearshore Hs, Tp, and MWD extracted from the lookup tables were interpolated to a 500

Table 1: Total water level records for 1980 through 2015. GOW2 station information includes node latitude, longitude, and depth.

Name	NOAA Tide Gauge Station	GOW2 Station	Hourly % Complete
North Beach Subcell, WA	Westport; Toke Point	47.0,-125.0; 650 m	96.0%
Netarts Littoral Cell, OR	Garibaldi; South Beach	45.5,-125.0; 1300 m	97.6%
San Francisco Littoral Cell, CA	San Francisco	38.0,-123.5; 1200 m	99.6%

m resolution for consistency across sites after an analysis testing interpolation to various resolutions (not shown) displayed this spacing adequately resolved the alongshore variation of the transformed wave conditions. Post-transformation to the nearshore, waves were linearly reverse-shoaled back to deep water before computing wave runup, similar to methodologies used in the Stockdon et al. [23] wave runup parameterization. Thus, any results using the term "alongshore-varying, nearshore wave height" refers to the linearly reverse-shoaled conditions. TWL_N were computed by adding the regional SWL to each alongshore-varying wave runup time series, producing a total of 46, 15, and 38 TWL_N time series along the WA, OR, and CA sites, respectively (Table 3).

In order to evaluate how the alongshore variation in beach topography affects TWLs, $TWL_{N\beta_Y}$ was computed by adding regional SWLs to $R_{2\%}$ calculated using alongshore-varying, nearshore waves (as described above) and a spatially-varying beach slope (β_Y). Estimates of beach slope every 5-10 m from the lidar surveys were averaged over 100 m bin spacing to avoid abrupt transitions between bins. Patterns in β_Y were similar across all study sites; beach profiles were the flattest towards the north of each cell and became steeper moving towards the south (Figure 2). WA contained the lowest sloping and least variable β_Y, while CA had the steepest and most variable β_Y of the three study sites (Figure 2). Due to differences in the alongshore resolution of the nearshore waves (500 m) and β_Y (100 m), $R_{2\%}$ was computed using β_Y and the closest alongshore-varying wave condition (Table 3). Any differences between TWL_N and $TWL_{N\beta_Y}$ are thus attributed to variation in beach slope, reflecting the influence of spatially-variable beach topography on TWLs.

Similar to the methodologies presented above, beach slope is generally estimated across a region based on a single lidar survey in time. However, variations in both the wave climate, water levels, and grain size across a coastline impose temporal variations in beach slope. In order to investigate how the temporal variability of beach slope affected TWLs, beach slopes were also extracted from profile data collected during monthly-to-quarterly topographic beach surveys (see Appendix B and Table Appendix B.1 for dates of surveys). The influence of temporally-varying beach slope (β_T) on TWLs, $TWL_{N\beta_T}$, was computed for 4, 19, and 7 profiles at WA, OR, and CA, respectively. A larger range of profiles were

Table 2: General SWAN specifications for lookup table generation for nearshore wave transformations at the three study sites. See Allan et al. [61] and Eshleman et al. [57] for complete descriptions of modeling methodologies and specifications.

Model Specifications	WA	OR	CA
SWAN Version	40.81 (3rd gen)	40.81 (3rd gen)	40.51 (3rd gen)
Grid Resolution	1000 m, 200 m	2000 m, 500 m, 100 m	500 m, 200 m
Wind	wind growth and quadruplet wave-wave interactions not included	wind growth and quadruplet wave-wave interactions not included	wind growth and quadruplet wave-wave interactions not included
Dissipation	includes whitecapping (Komen formulation) and bottom friction (JONSWAP formulation)	includes whitecapping (Komen formulation) and bottom friction (JONSWAP formulation)	includes whitecapping (Janssen formulation) and bottom friction (Madsen formulation)
Modeled Conditions	2194	2184	4577

Table 3: Description of wave and beach slope inputs to TWL computations.

Variable	Waves	Beach Slope	No. Transects per Site
TWL_R	shelf edge, deep-water	regional estimate; β_R	1 per site
TWL_N	nearshore-transformed and linearly reverse-shoaled (500 m resolution)	regional estimate; β_R	46 for WA 15 for OR 38 for CA
$TWL_{N\beta_Y}$	nearshore-transformed and linearly reverse-shoaled (500 m resolution)	spatially-varying; β_Y (100 m resolution)	217 for WA 71 for OR 160 for CA
$TWL_{N\beta_T}$	nearshore-transformed and linearly reverse-shoaled (closest to beach profile)	temporally-varying; β_T	4 for WA 19 for OR 6 for CA

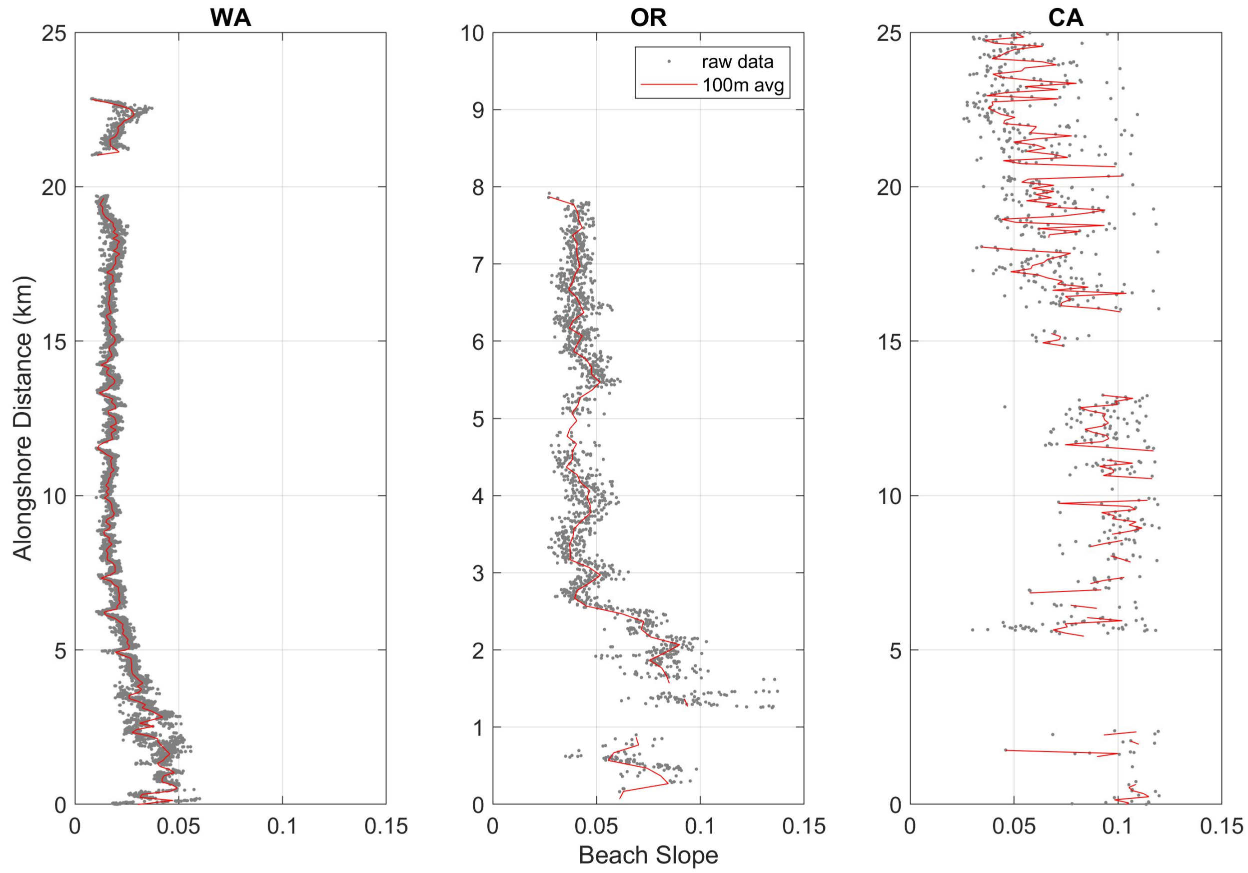

Figure 2: Spatially-varying beach slope extracted from lidar data at the North Beach subcell (WA), Netarts Littoral Cell (OR), and San Francisco Littoral Cell (CA). Grey dots are representative of all lidar-extracted beach slopes, while the red line displays the data smoothed to the 100 m resolution used in the analysis.

included in OR due to the shorter temporal record (see Table Appendix B.1). $TWL_{N\beta_T}$ were only computed for the record length of beach slope measurements. For example, CA surveys began in 2004, so TWLs were only computed over the time period of 2004 - 2015. Extreme $TWL_{N\beta_T}$ were specifically calculated by finding the closest surveyed beach slope for every day in time and computing the $R_2\%$. Estimates of $R_2\%$ were added to the regional SWL to produce $TWL_{N\beta_T}$ time series and then the 10-largest TWL events were extracted every year. $TWL_{N\beta_T}$ therefore represents the seasonality in both the wave climate and the beach slope.

2.4. Extracting Extreme Total Water Levels and Their Corresponding Impacts

Our analysis investigates the influence of shelf bathymetry and beach topography on extreme TWLs. Here "extreme" is defined using the r-largest method [72], where r is equal to the 10-largest TWL events in a given year, for a total of approximately 350 extreme TWL events in each 35 year record. TWL_N, $TWL_{N\beta_Y}$, and $TWL_{N\beta_T}$ were calculated at numerous alongshore locations, based on the spatial variability of the morphologic variables, thus providing multiple extreme TWL time series per study site (Table 3). Results of the magnitude of TWL_N and $TWL_{N\beta_Y}$ were averaged at each study site in order to compare to TWL_R. In order to test if extreme TWL_N or $TWL_{N\beta_Y}$ occurred during the same storm events as extreme TWL_R, the offshore waves components of the nearshore waves driving extreme TWL_N and $TWL_{N\beta_Y}$ were compared to the offshore waves driving TWL_R.

The collision regime of the Sallenger Storm Impact Scale [73, 74] was used to assess the exposure of each location to extreme TWLs. The collision regime, a proxy for erosion, occurs when the elevation of the TWL reaches or exceeds the elevation of the dune/bluff/structure (hereinafter dune) toe. A regionally-uniform dune toe elevation of 5.1 m, 4.8 m, and 4.6 m, for WA, OR, and CA, respectively, was computed for each study site by averaging each location's dune toe extracted from morphology data. The regional average dune toe contour was used to compute how often extreme TWLs fell within the collision regime in each location.

The spatially-varying impacts driven by extreme $TWL_{N\beta_Y}$ and TWL_N at each study site were computed by calculating the percent of coastline falling within the collision regime. Extreme TWL_N and $TWL_{N\beta_Y}$ (N = 350 for each) were computed at all transects representing both the alongshore-varying waves (every 500 m) and β_Y (every 100 m). The metric, "percent of coastline within the collision regime" was calculated by assessing the uniformity of the coastal response for all 350 events per transect, per site. If one of the 350 extreme TWLs fell within the collision regime at all transects in a study site, then 100% of the coastline would fall within the collision regime for that event (Figure 3). If one of the 350 extreme TWLs did not reach the dune toe across any of the coastline, then 0% of the coastline would fall within the collision regime. A "partial" impact of the coastline during an event occurred when some transects fell within the collision regime, while others did not. For example, if there were 10 transects across a study site and 4 of them fell within the collision regime, than 40% of the coastline would be impacted by that event (Figure 3). The percent of coastline within the collision regime was calculated for all 350 events to find the distribution of events that caused partial, full, or no collision at each study site. The same metric was calculated using impact hours per year (IHPY), where instead of measuring the impact of extreme TWLs, the amount of time (in hours) that the coastline was in full, partial, or no collision regime was computed. IHPY were defined as the number of hours on record that the elevation of the TWL reached or exceeded the elevation of the regionally-averaged dune toe contour.

2.5. Evaluating Hypothetical Alternative Futures

Once the influence of topography and shelf bathymetry on coastal TWLs is explored, our analysis focuses on understanding how future changes to the wave climate may alter coastal TWLs. A range of potential future wave climates were characterized using hypothetical distribution shifts to the deep-water historical records of wave height, period, and direction at each site. Once the average change in each variable was added to the deep-water historical record, the record was transformed to the nearshore using the lookup tables. This approach allows for an efficient manner of investigating the impact of changes in wave forcings without the computational demands of downscaling global climate model ensemble members at each

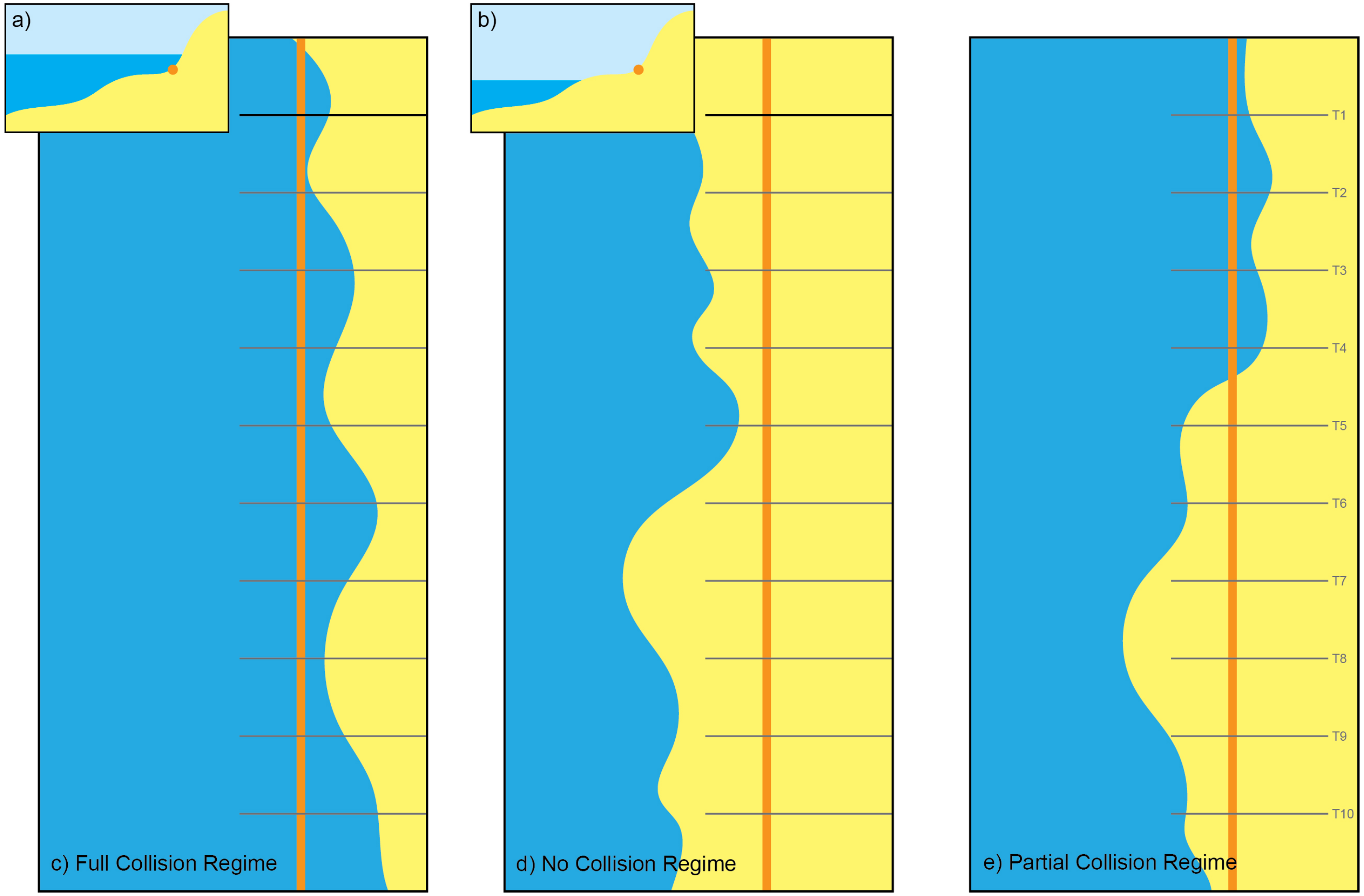

Figure 3: Cross-section view of example transect (T1, highlighted in black in panels c and d) during a) collision (e.g., TWL $\geq$ dune toe) and b) no collision (e.g., TWL $<$ dune toe), where the orange circle represents the dune toe, blue represents the TWL, and yellow represents the beach. Plan view schematic of c) full, d) no, and e) partial collision regime. Here, blue represents the TWL, yellow is the beach, and the orange line represents the dune toe contour. Grey lines represent transects where spatially-variable TWLs are computed. Full collision regime occurs when a TWL event impacts all transects at a study site (c), no collision regime occurs when a TWL event does not impact the dune toe at any transect (d), and partial collision regime occurs when a TWL event impacts some but not all of the transects (e).

location. Due to the uncertainty surrounding projections of future storm tracks and intensities, we investigate scenarios surrounding projections in the literature (e.g., [42, 39, 40]; usually between a ± 2 to 10% change from present, depending on variable), as well as scenarios outside the range of current projections (e.g., ± 10 to 20% change from present). While less likely, the hypothetical scenarios at the higher end of this range are used to consider more extreme projections of changes to the wave climate and are meant to be viewed as a means of exploring relative impacts at each location.

By mid-century, projected increases to mean sea level between 15 cm and 30 cm will likely overwhelm changes in the magnitude of TWLs driven by changes to the wave climate [31]. The effect that future changes to the wave climate may have on TWLs and their associated impacts are therefore contextualized by comparing results to TWLs computed with a maximum increase/decrease of mean sea level by 30 cm, where an average increase (decrease) to the water level at intervals between 6 cm and 30 cm are added (or subtracted) to existing still water levels. A sea level rise of 30 cm is more likely than not by mid-century, and highly-likely by the end of the century [75, 76], while comparing to negative sea level assesses how the relationship has changed over the last several century, when sea level was lower than present.

Changes to the climate alone, however, are not the sole drivers of coastal change. Mills et al. [51] demonstrate that human modifications to the coastal system may alter the coastline more than climate change, especially by mid-century. Two scenarios describing the most common coastal protection strategies are investigated: coastal armoring (hard) and beach nourishment (soft). Coastal armoring (e.g., sea walls, rip rap revetments, etc.) prevents dune or bluff erosion but cuts off the local sediment supply to the beach, generating local erosion and potentially steepening beach slopes, whereas beach nourishment replenishes the sediment supply, flattening the beach. To begin to explore the role coastal management adaptations may have on future TWLs, we use beach slopes as proxies of coastal management techniques at each location, and allow beach slopes to steepen and flatten by a maximum/minimum of 0.01 relative to present-day conditions. This value represents a -20 to 20% change in aggregated beach slope across all study sites in order to explore a uniform change in beach slope.

Hypothetical shifts to the average variables (i.e., wave height, wave period, wave direction, beach slope, sea level rise) were changed independently of one another to allow for the comparison of effects within and between locations. We primarily considered percent change in impacts (rather than absolute) from present-day within each study site to reflect the significance of the impact relative to each place as a whole, allowing for an easier comparison across locations.

3. Results

In order to quantify how a change to the offshore wave climate may alter local coastal hazards, the influence that shelf bathymetry and beach topography have on the magnitude of extreme TWLs at each location must first be understood. TWL time series were therefore calculated using various combinations of spatially and temporally-varying nearshore waves and beach slope (see section 2.3 for a complete description of methods and Table 3 for abbreviation references). Once the control of morphology on the magnitude of TWLs is understood, our results focus on the resultant impacts of extreme TWLs at each study site, now and into the future.

3.1. The Influence of Shelf Bathymetry on the Magnitude and Drivers of Extreme Total Water Levels

The 10 largest extreme TWL_R events every year (N = 350) average (standard deviation) 5.0 m (0.36), 5.4 m (0.47), and 5.1 m (0.48) in WA, OR, and CA, respectively (top panel, Figure 4). Extreme TWL_R in WA and OR arrive from approximately 255° and 260°, for WA and OR respectively, slightly southwest of shore-normal. In contrast, extreme TWL_R in CA are driven by waves arriving from predominantly the northwest (on average 285°). The majority of waves driving extreme TWL_R across all locations have periods between 15 - 20 s and wave heights between 3 - 8 m. The average wave height driving TWL_R in CA is approximately 1 m lower than the average wave height driving TWL_R in WA or OR,

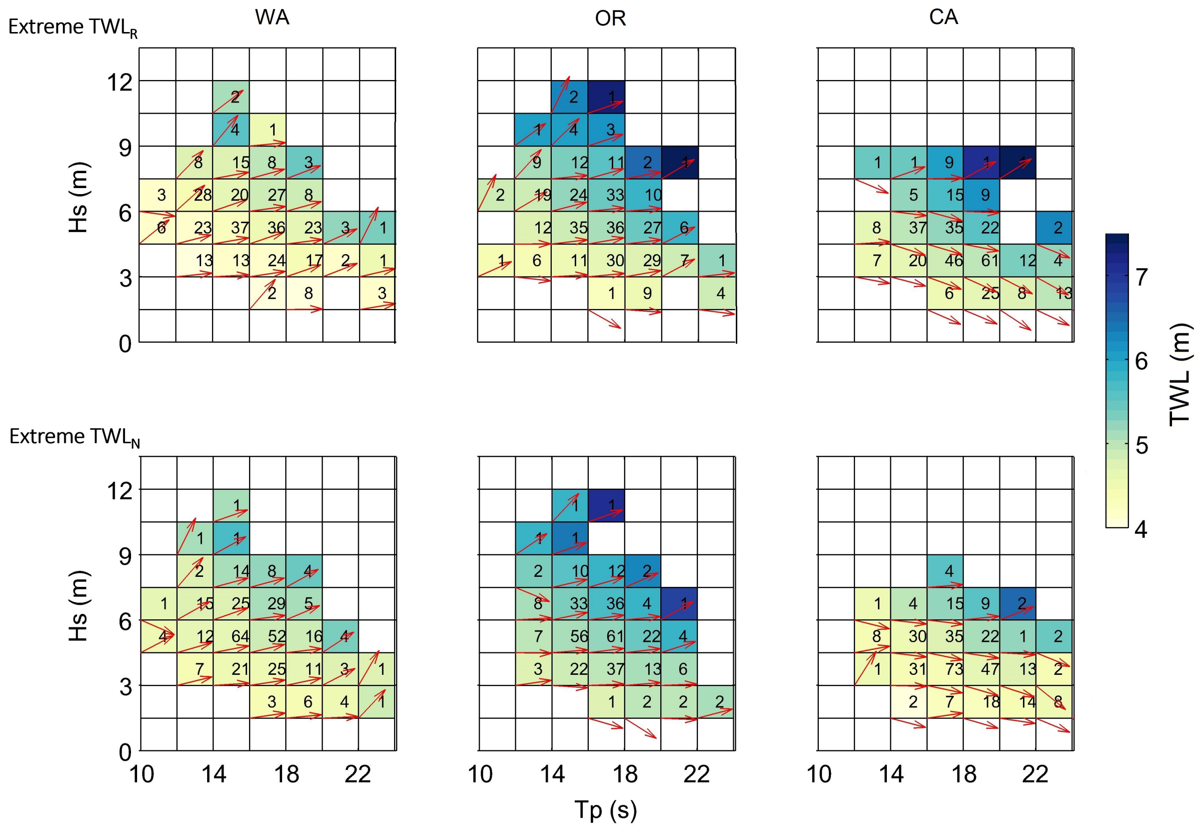

Figure 4: Extreme total water levels at each study site computed using offshore, deep-water waves and a uniform beach slope (TWL_R; top panel) and alongshore-varying nearshore waves (linearly reverse-shoaled) and a uniform beach slope (TWL_N; bottom panel). Each grid cell displays the offshore, deep-water wave conditions driving the 10 largest TWL events every year regardless of computation technique (e.g., alongshore-varying nearshore are matched to their offshore forcings), binned by wave height (Hs) and peak period (Tp). The red arrows depict the mean wave direction of the conditions within each grid cell, and begins in the lefthand lower corner of the corresponding cell. The numbers in each grid represents the number of extreme TWL events that are classified in that grid cell (an average for TWL_N), while the colorbar represents the average magnitude of the TWL within each cell.

however, the $R_{2\%}$ contributes to approximately 60% of the magnitude in CA, compared to 40% and 50% for WA and OR, respectively.

Once wave transformation to the nearshore is taken into account, the average magnitude of extreme TWL_N is slightly less than TWL_R across all locations (4.8 m, 5.3 m, and 4.7 m for WA, OR, and CA, respectively). The difference between the maximum TWL_R and maximum TWL_N at each transect varies by approximately 20-40 cm across all study sites (Figure 5). The difference between the median TWL_R and median TWL_N at each transect is slightly less. The largest differences between the magnitude of extreme TWL_N and TWL_R occur in CA. Once transformed to the nearshore and linearly reverse-shoaled, the wave heights that generate the 10 largest extreme TWL_N every year are on average 23% smaller than the wave heights that generate TWL_R in CA, a consequence of wave shoaling and refraction. This is also reflected in the decrease in the $R_{2\%}$ by 14% (Table 4). CA is also the only location that experiences amplification of TWL_N, where the alongshore-varying TWL_N can be greater than TWL_R (Figure 5). Wave conditions in WA and OR are less affected by wave shoaling and refraction over the shelf (e.g., wave height decreases and wave direction shifts slightly less) compared to CA (Table 4).

At all study sites, at least 15% of the wave events that drive the 350 extreme TWL_R per year occur at different times than the wave events driving extreme TWL_N at any given coastal transect (Figure 6). This means that when comparing differences between the deep-water conditions driving extreme TWL_N and TWL_R at each study site, anywhere from 40 - 90 of the selected 350 events per transect are found to occur on different days. The difference in the largest extreme events per TWL calculation slightly modifies the average wave conditions forcing TWL_N (Table 4). For example, the average deep-water wave direction shifts slightly northward in WA and OR (260° and 265°, respectively), while in CA, the average deep-water wave direction shifts southward, arriving from 278° (bottom panel, Figure 4). Therefore, when including wave transformation processes into TWL computations, extreme TWL_N are driven by a different offshore wave climate (arriving from slightly more north for OR and WA and slightly more south for CA) compared to deep-water conditions driving TWL_R. Many of the highly oblique deep-water wave conditions (top panel, Figure

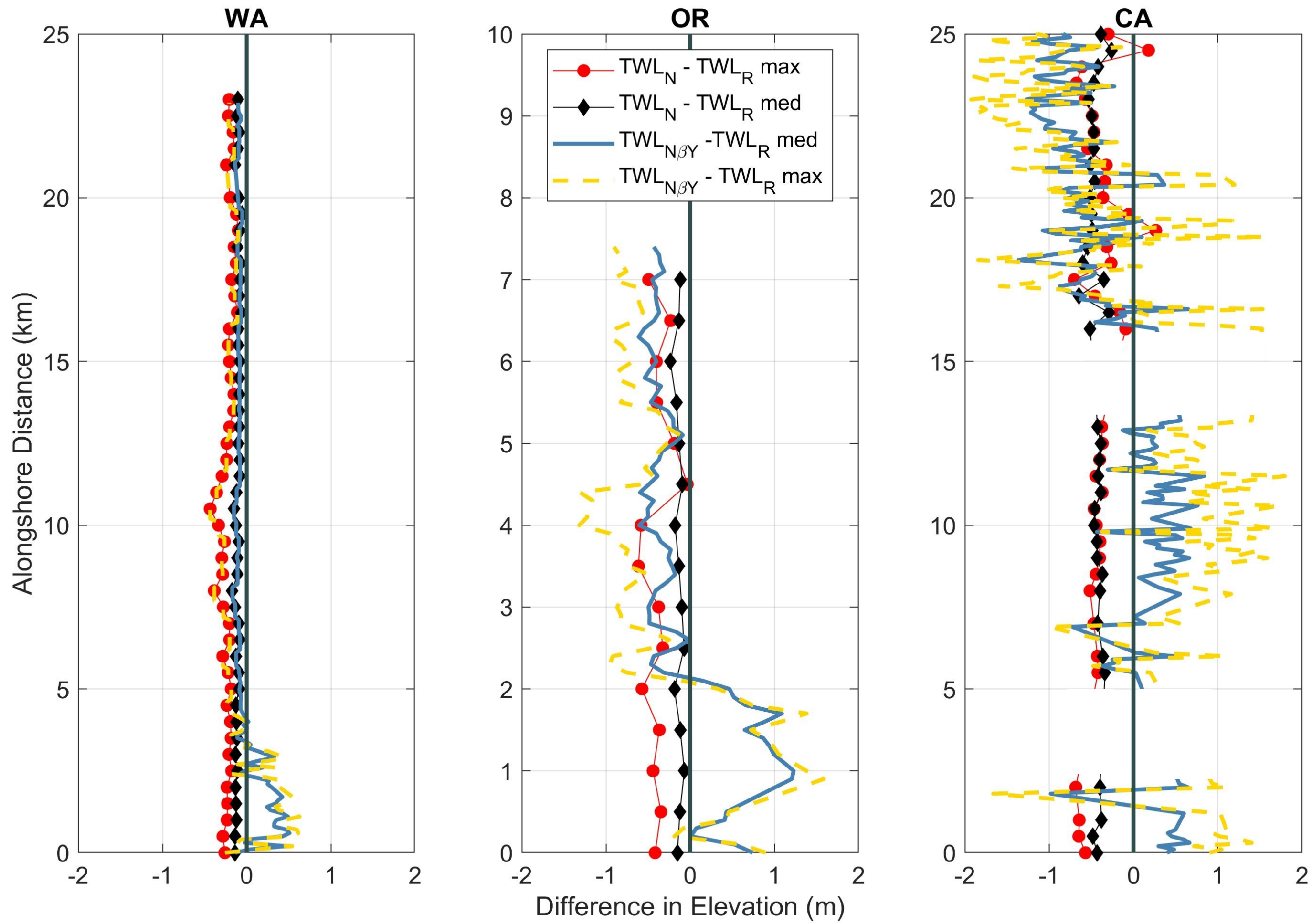

Figure 5: The difference in elevation between the median and maximum TWL_N at each transect and regional TWL_R (black and red symbols, respectively) and difference in elevation between the median and maximum $TWL_{N\beta_Y}$ at each transect and regional TWL_R (blue solid and gold dotted lines, respectively) per study site.

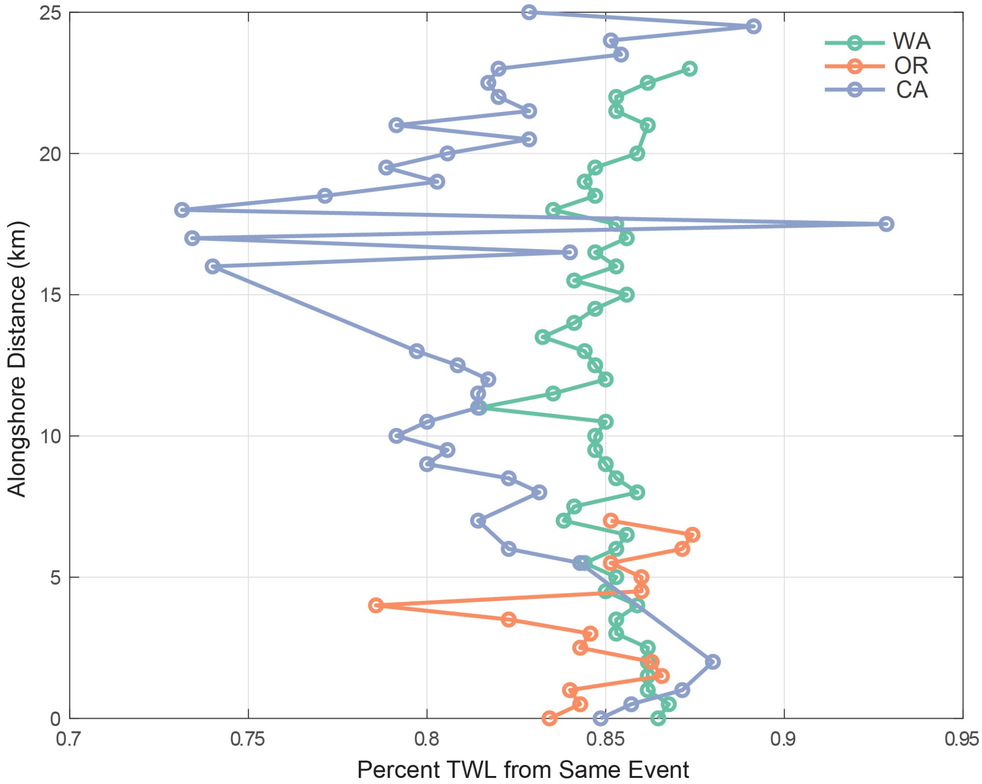

Figure 6: Percent of extreme TWL_N driven by the same offshore conditions as extreme TWL_R at each alongshore-varying, nearshore wave node. Colors are representative of the three different locations.

4) do not show up in the deep-water events driving TWL_N (bottom panel, Figure 4), where wave conditions arriving from slightly more shore-normal are favored. Again, CA is the most affected by this process, where both the offshore, deep-water wave conditions driving TWL_N are the most dissimilar to offshore, deep-water wave conditions driving TWL_R and the nearshore transformed wave conditions are altered the most (Table 4). Thus, not only are wave heights and directions altered by shoaling and refraction, impacting the magnitudes of TWLs, but the event driving extreme coastal TWLs may be different when taking into account wave transformation processes.

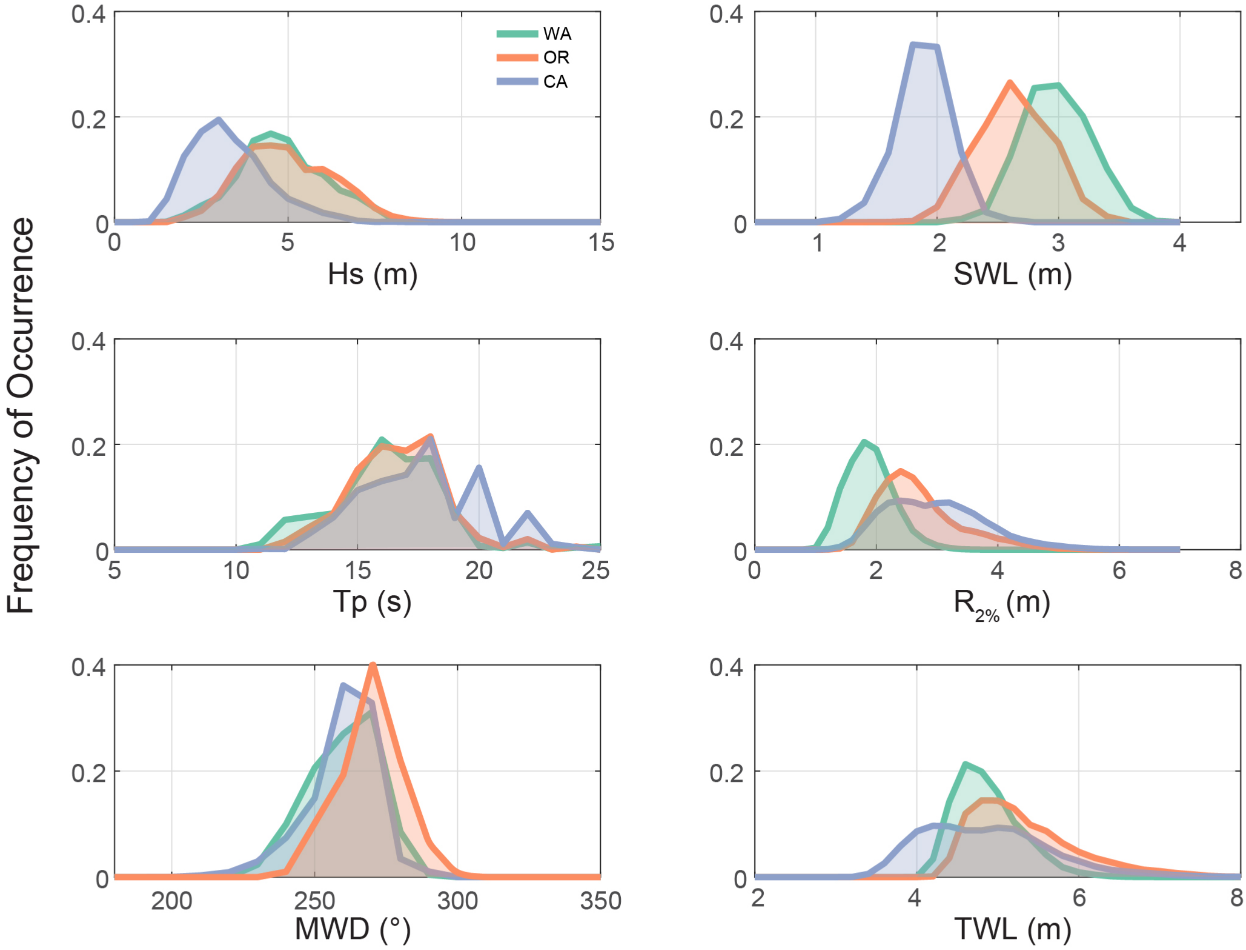

Figure 7: Distributions of the magnitude of wave height (Hs), peak period (Tp), direction (MWD), wave runup ($R_{2\%}$), and still water levels (SWL) driving extreme $TWL_{N\beta_Y}$ events for all transects at each study site. Colors represent each location where the WA, OR and CA are green, orange, and blue, respectively. Each distribution encompasses the spatially-varying $TWL_{N\beta_Y}$ at each specific study site.

Table 4: The average percent change between the conditions driving extreme TWL_R computed using offshore, deep-water waves and β_R and both the offshore, deep-water and nearshore-transformed wave conditions driving extreme TWL_N using β_R. For example, row 4, column 2 depicts the average percent change between the offshore, deep-water wave height conditions driving TWL_R and the offshore, deep-water wave height conditions driving TWL_N (-2.5%) and the average percent change between the offshore, deep-water wave height conditions driving TWL_R and the nearshore-transformed wave height conditions (linearly reverse-shoaled) driving TWL_N (-13.3%) in WA. The former represents differences in offshore forcings, while the latter represents wave transformation and shoaling processes. Wave direction is represented by a percent change over a 360° scale.

Variable	WA	OR	CA
TWL	-2.8/-2.0%	-3.9/-2.8%	-8.6/-8.6%
R2	0/-4.1%	-1.1/-5.0%	-1.9/-14.0%
Hs	-2.5/-13.3%	-1.6/-11.7%	-3.0/-26.0%
MWD	1.5/2.0% shift north	1.9/3.8% shift north	-2.5/-8% shift south

3.2. The Influence of Spatially-varying Beach Slope on the Magnitude and Drivers of Extreme Total Water Levels

Extreme $TWL_{N\beta_Y}$, computed using both alongshore-varying nearshore waves and β_Y, has the highest magnitude in OR and a similar magnitude in CA and WA. Averaged across the cell, comparisons between the magnitudes of TWL_R, TWL_N, and $TWL_{N\beta_Y}$ are similar. However, the inclusion of β_Y shows that using TWL_R would underpredict the elevation of the TWL by up to 1.8 m in some locations (Figure 5). The specific storm events driving extreme $TWL_{N\beta_Y}$ compared to the events driving extreme TWL_N are similar, thus the driving processes of local TWLs are defined by wave transformation over the shelf rather than local estimates of beach slope. The conditions driving extreme $TWL_{N\beta_Y}$ include wave heights ranging from 1.0 to 9.7 m, peak periods ranging from 10.5 to 24.5 s, non-tidal residuals ranging from -0.35 to 0.90 m, and still water levels ranging from 0.7 to 3.8 m (Figure 7). While this broad range of driving conditions is mostly the same as the range of conditions driving TWL_N, the variance of extreme $TWL_{N\beta_Y}$ increases across all locations.

When incorporating the spatial variability of nearshore waves and beach topography in TWL computations, OR and CA are most controlled by the magnitude of $R_{2\%}$, while extreme $TWL_{N\beta_Y}$ in WA are driven by high still water levels. CA has the lowest magnitude still water level and wave height of all locations, but the largest contributions from $R_{2\%}$, due to a longer average wave period and the steepest beach slopes of all three study sites (Figure 7). Regionally, the largest waves occur in OR and paired with relatively steep beach slopes and high still water levels, so do the largest magnitude $TWL_{N\beta_Y}$. On the other hand, while WA experiences waves as large as those in OR, high still water levels coinciding with low beach slopes drive less of a contribution from $R_{2\%}$ for extreme $TWL_{N\beta_Y}$ (Figure 7).

3.3. The Influence of Temporally-varying Beach Slope on the Magnitude and Drivers of Extreme Total Water Levels

The standard deviation of β_T for each beach profile is positively correlated to the individual profile's average beach slope. The steeper the average β_T, the larger the variability to β_T over time (top panel, Figure 8). Individual profiles with an average beach slope greater than 0.04 generally have standard deviations greater than 0.01, while beach slopes less than 0.03 have standard deviations less than 0.005.

The range of the magnitude of extreme $TWL_{N\beta_T}$ is lower for profiles where the standard deviation of β_T is less than 0.005 than for profiles with standard deviations of β_T greater than 0.005. The magnitude of extreme $TWL_{N\beta_T}$ computed on profiles where the standard deviation of the beach slope is greater than 0.005 ranged over 3 m, while profiles with standard deviations less than 0.005 have ranges of extreme $TWL_{N\beta_T}$ less than 2 m (bottom panel, Figure 8). Thus, the temporal variability of beach slope likely plays a larger role in influencing TWLs on steep beaches. Due to the dependence of the Stockdon et al. [23] $R_{2\%}$ parameterization on beach slope, the magnitude of extreme $TWL_{N\beta_T}$ occurring on steep profiles varies across a larger range of beach slopes, while $TWL_{N\beta_T}$ occurring on shallow profiles exhibits less variability and can be better characterized by simply using the average beach slope of the profile. That being said, the steeper beaches in our study sites (e.g., OR and CA) experience a corresponding variability in β_Y. Therefore, incorporating β_T into TWL estimates may be more important on steep sections of overall flatter coastlines (e.g.,

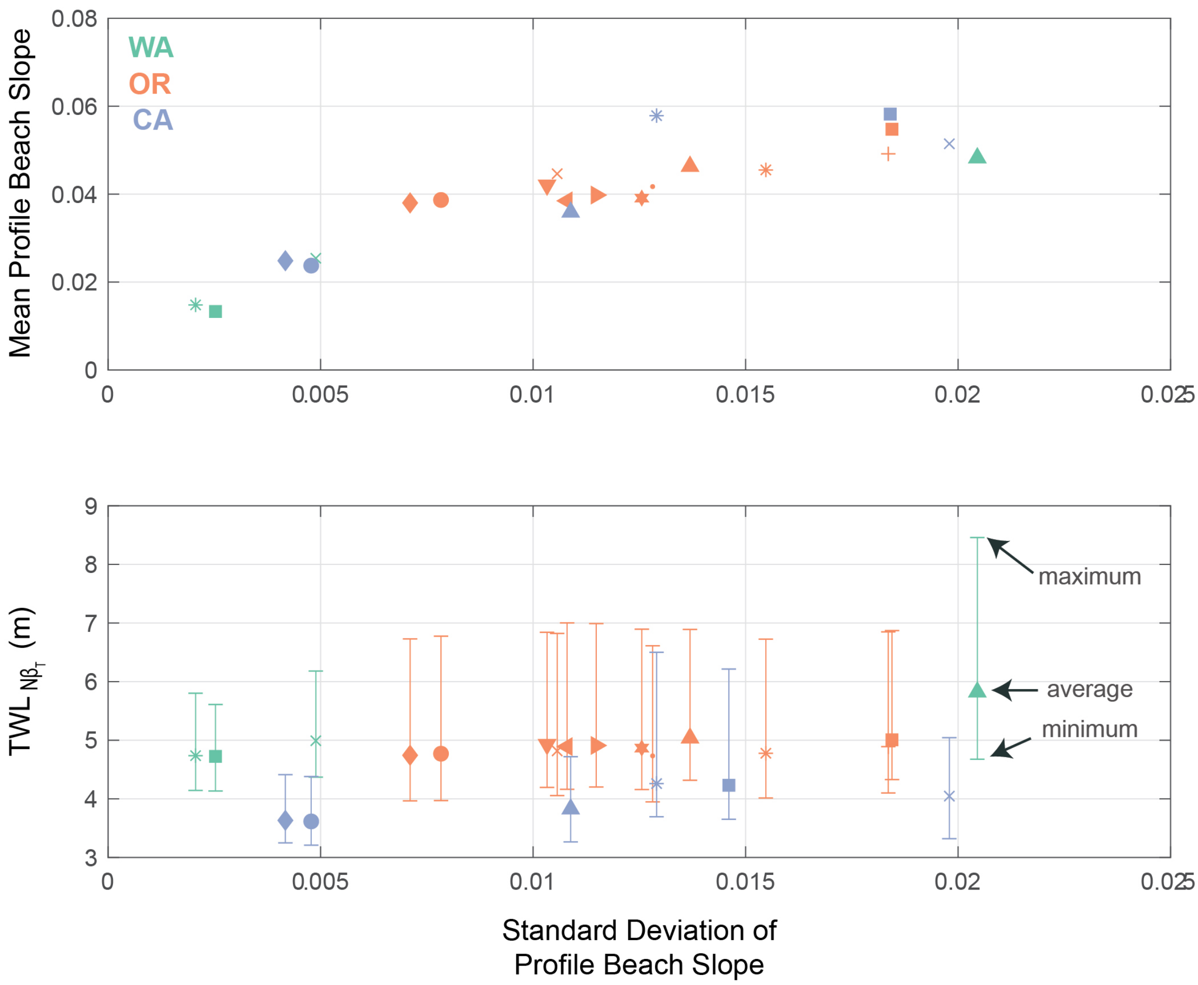

Figure 8: Top panel) The relationship between the standard deviation of β_T for a specific profile versus the average β_T of that same profile. Bottom panel) Variability in extreme $TWL_{N\beta_T}$ at each profile, where the symbol indicates the average magnitude $TWL_{N\beta_T}$ and the whiskers denote the maximum and minimum $TWL_{N\beta_T}$. Distinct profiles are denoted by different symbols and colors represent the three locations, where green is WA, orange is OR, and blue is CA, consistent across both plots. Only 12 of the 19 OR profiles are displayed but they cover the representative variability of TWLs.

the steeper, southern section of WA), where β_Y does not properly define the true range of beach profile variance at the location.

3.4. Analyzing the Local Impacts of Total Water Levels - Present-day

While understanding the magnitude of extreme TWLs and how they differ between locations is important, the subsequent impact to coastal habitat or infrastructure due to variations in the magnitude of the TWL is more relevant for describing the local effects of larger-scale phenomena. Impacts are often assessed based on events meeting or exceeding some threshold. Thus, small changes to the magnitude of extreme TWLs can have large repercussions to impacts at a specific location. When the influence of shelf bathymetry on TWLs is is taken into account, the majority of TWL_N events drive either the entirety (100%) or none (0%) of the coastline to be within the collision regime at all study sites (Figure 9). Approximately 1/3 of the 350 TWL_N events in CA partially impact the coastline at once (e.g., 5 to 90% of the coastline falls within the collision regime during specific events rather than 0% or 100% of the coastline). This value is less for WA and OR. The distribution of impacts becomes more varied when including beach topography in TWL calculations, and $TWL_{N\beta_Y}$ are found to drive more partial impact of the coastline. For example, 3/4, 1/2, and almost all of $TWL_{N\beta_Y}$ events partially impact the coastline in WA, OR, and CA, respectively.

In WA, the majority of extreme $TWL_{N\beta_Y}$ events impact 1/4 or less of the coastline at once, and only 1/10 of $TWL_{N\beta_Y}$ events impact 100% of the coastline. In contrast, 100% of the coastline in OR falls within the collision regime during almost half of the extreme $TWL_{N\beta_Y}$ occurring on record (Figure 9). CA's exposure to the collision regime is more spatially variable than that of WA and OR, where extreme $TWL_{N\beta_Y}$ most frequently impact 40 to 60% of the coastline at once, while only very few extreme $TWL_{N\beta_Y}$ impact 90% or more of the coastline at once (Figure 9).

At least some portion of the OR and CA coastline falls within the collision regime during all extreme $TWL_{N\beta_Y}$ events. Thus, impacts occurring more frequently are explored by using the metric impact hours per year (IHPY, [77, 30, 25]). While the majority of conditions

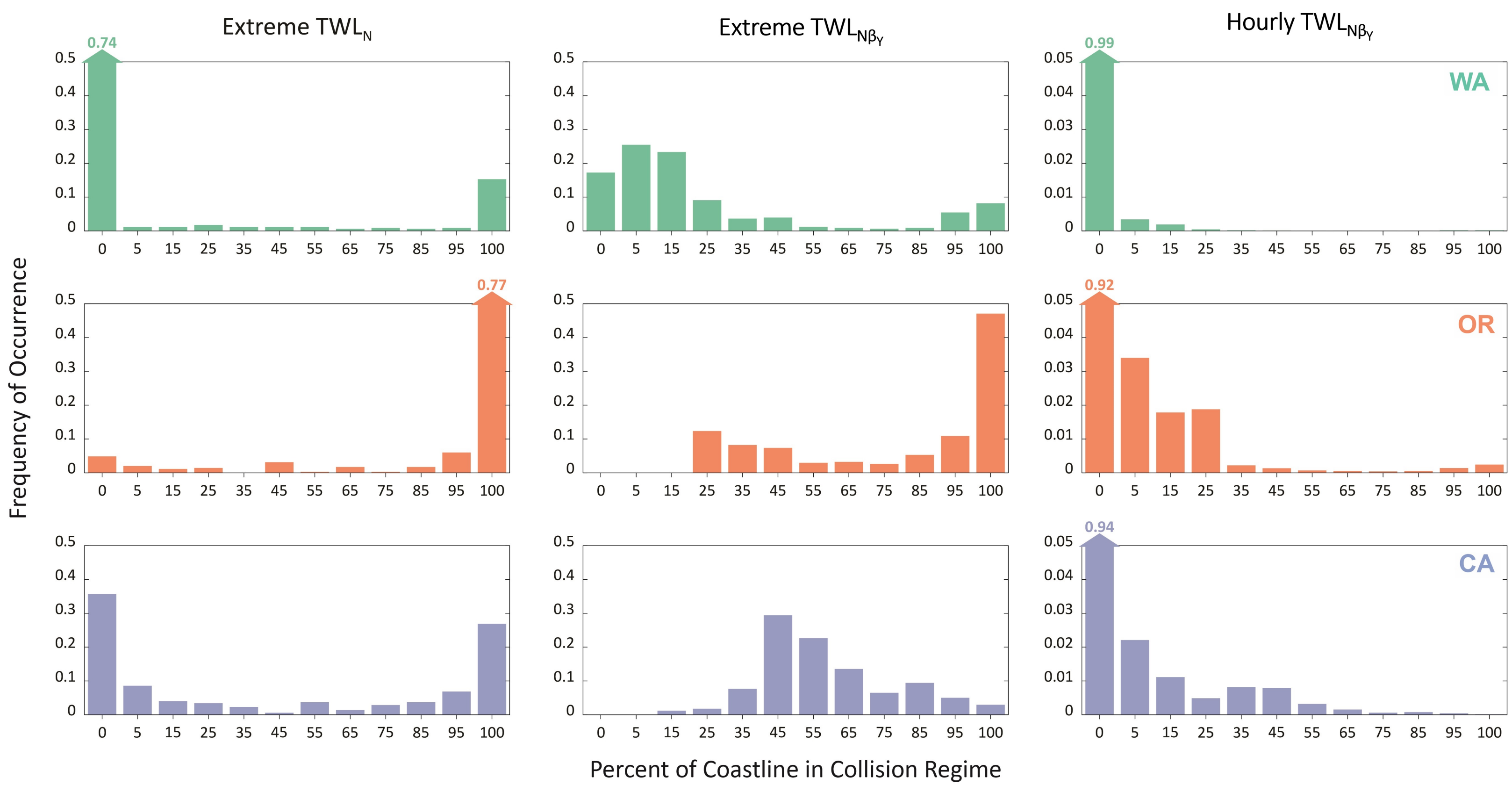

Figure 9: Percent of coastline falling within the collision regime during the left panel) 10 largest TWL_N events each year, middle panel) 10 largest $TWL_{N\beta_Y}$ events each year, and right panel) hourly $TWL_{N\beta_Y}$ events. Colors represent different locations where green is WA, orange is OR, and blue is CA. Values extending off the plot are indicated the number above the bar.

drive no IHPY (e.g., bar 0, right hand side in Figure 9), 0.6%, 9% and 7% of hourly TWLs are above the dune contour in some location along each stretch of coastline in WA, OR, and CA, respectively. This analysis portrays OR to be in the collision regime slightly more often than WA or CA in any given year.

3.5. Analyzing the Local Impacts of Total Water Levels - Future

The above sections provide evidence that the transformation of wave conditions over shelf bathymetry and beach topography are important to consider when estimating the local magnitude and resulting impacts of TWLs on sandy coastlines. Therefore, exploring how offshore changes to the deep-water wave climate may propagate to the nearshore is essential for understanding a community's exposure to future coastal hazards. Here we only model changes to conditions forcing $TWL_{N\beta_Y}$ due to the previously described influence of both shelf bathymetry and beach topography on driving conditions of TWLs and their resulting impacts.

The magnitude and resulting impact of $TWL_{N\beta_Y}$ is positively correlated with changes in wave height, peak period, beach slope, and sea level; during positive changes, TWLs increase at each location and during negative changes, TWLs decrease at each location. A clockwise (positive) shift (more waves arriving from the north) in wave direction slightly increases the magnitude $TWL_{N\beta_Y}$ in WA and OR and decreases the magnitude of $TWL_{N\beta_Y}$ in CA, while an anticlockwise (negative) shift (more waves arriving from the south) in wave direction has the opposite effect. While all locations display similar trends in changes to impact hours driven by hypothetical shifts to wave height and wave period, CA is most sensitive to changes to the wave climate (Figure 10). For example, a counterclockwise rotation of mean wave direction drives changes of similar magnitude to that of changes to wave height in CA, while shifts in mean wave direction drive relatively small variability in TWL magnitude or impacts in WA or OR (Figure 10).

Overall, changes to the wave period alter impact hours the most: a lengthening of the average wave period by just 5% (the upper end of projections in the literature) results in a greater than 20% change in IHPY at all locations. This means a 0.5 - 1 s increase to the

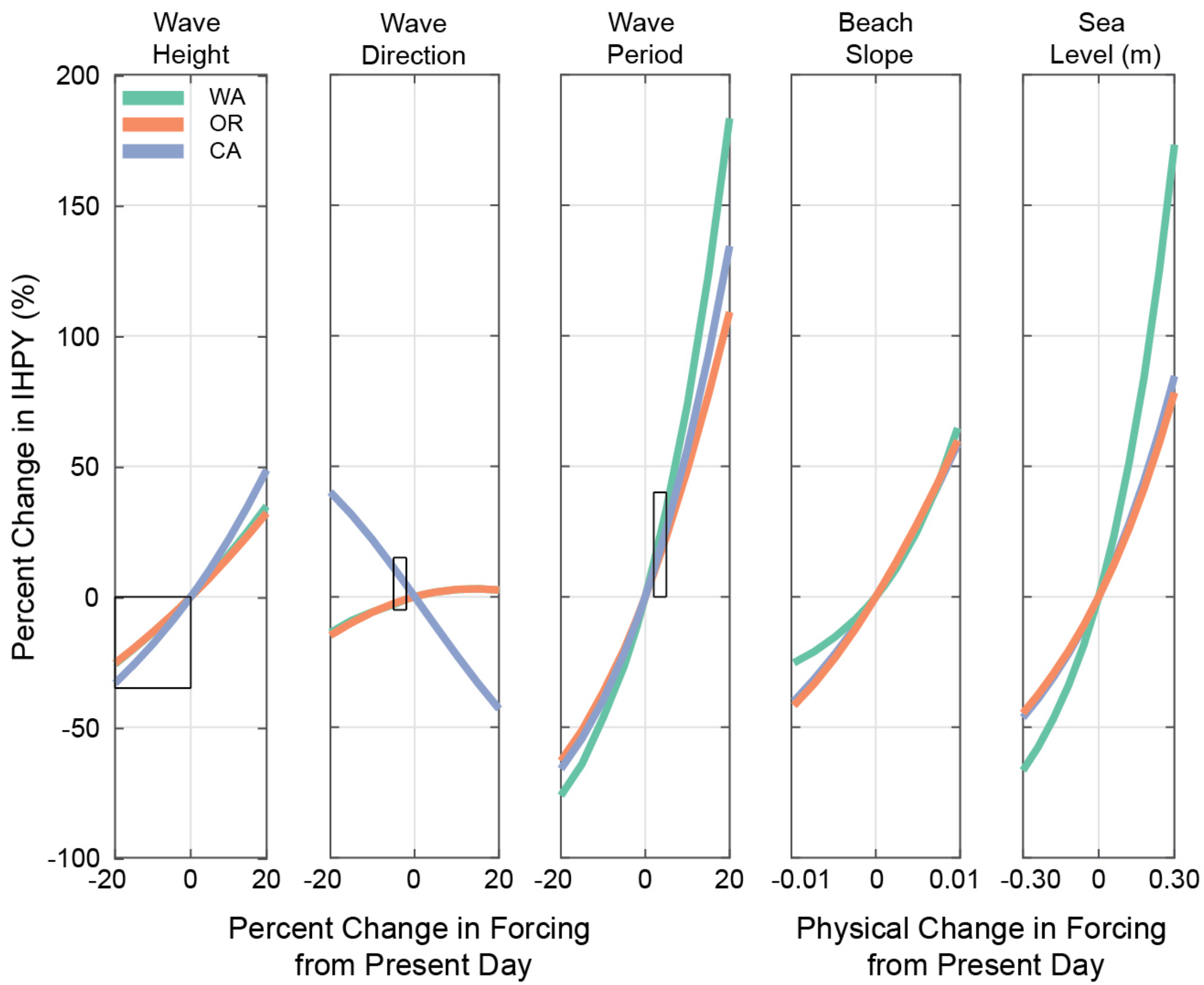

Figure 10: Percent change in Impact Hours Per Year (IHPY) due to hypothetical future climate change scenarios of the wave climate, as well as the physical change in IHPY for future scenarios of beach slope and sea level at each study site. The boxes in panels 1 - 3 represent the approximate percent change in wave height, period, and direction projected by [40, 39] and [42]. Colors represent different locations where green is WA, orange is OR, and blue is CA.

average wave period would have a similar effect on the coastline as a 50 cm (approximately 20%) increase of the wave height. The variable driving the second largest modification to IHPY is a change in mean sea level. An increase in mean sea level as small as 30 cm increases IHPY by 85%, 78%, and 173% in CA, OR, and WA, respectively. All three locations are affected by increases to the beach slope similarly, however, OR and CA have the most reduced IHPY from beach flattening. Overall, changes to the beach slope alters impacts more than a change in wave height or direction at all locations, and almost as much as a 30 cm increase in sea level at OR and CA.

4. Discussion

Overall, both wave transformation over shelf bathymetry and beach topography are integral components for properly assessing the magnitude and impacts of local coastal TWLs. Wave transformation processes effect coastal TWLs because there is a difference in 1) the conditions that drive extreme TWL_R and TWL_N and 2) the magnitude of TWL_N compared to TWL_R. Specific wave conditions transforming from deep-water to the nearshore may be physically altered due to shoaling, refraction, and/or dissipation such that they no longer necessarily drive the most extreme TWLs at a specific location. For example, oblique waves refracting over a canyon could divert wave energy, generating a shadow zone, thus, lowering nearshore wave heights. This study shows that at least 15% of the storm events driving extreme TWL_N are different than the events driving TWL_R at all locations. For example, the average wave direction of the offshore events driving TWL_N compared to TWL_R shift towards the south by 7° in CA, whereas the average wave direction of the nearshore events driving TWL_N compared to the offshore conditions driving TWL_R shift 25° towards the south due to refraction (Table 4). While specific alongshore variations in the transformed wave climate at each site may exist, on average, extreme TWL_N are preferentially driven by shore-normal offshore waves that are unlikely to undergo large transformations across the shelf.

The overall influence of wave transformation processes on TWLs at a specific location depends on the amount of shoaling and refraction waves undergo over shelf bathymetry, as well as the relative contribution of the $R_{2\%}$ to the TWL. TWLs in WA are the least influenced by wave transformation over shelf bathymetry compared to all study sites, even though the waves driving extreme TWL in WA are slightly more affected by wave transformation over shelf bathymetry compared to wave conditions driving extreme TWLs in OR (e.g., TWL_N is 2% and 2.8% less than TWL_R in WA and OR, respectively, while wave height is 13.3% and 11.7% less than wave heights driving TWL_R in WA and OR, respectively (Table 4). While the shelf bathymetry is more complex at the WA study site than the OR study site, the lack of a large resulting impact from wave transformation to the magnitude of extreme TWLs at WA is due to the composition of extreme TWL events. TWLs at WA are comprised of high still water levels, which are driven by a large tidal range and large storm surges [27], resulting in less contribution of $R_{2\%}$ to TWLs. This contribution is further reinforced by the shallow beach slopes at WA, due to fine sands across a progradational setting [54]. Thus, while wave transformation occurs across all sites, the relative contribution of the $R_{2\%}$ to the TWL controls how much wave transformation processes effect coastal TWLs.

Alternatively, CA is the most influenced by wave transformation processes over nearshore shelf bathymetry due to the complex offshore setting, as well as the importance of the contribution of the $R_{2\%}$ to TWLs. The region's steeper beach slopes and on average longer period waves make the $\mathrm{R}_{2\%}$ the largest contributor to extreme TWLs. Thus, any wave transformation across the shelf will influence this location more than one where the still water level dominates extreme TWLs. The largest waves arrive during the winter from the North Pacific [78] and this is displayed by the predominant direction of waves during extreme TWLs. However, the deep-water conditions driving extreme TWL_N shift 7° towards the south compared to the deep-water wave conditions driving TWL_R. Offshore features such as Point Reyes and the Farallon Islands may block or refract wave energy arriving from the north, thus changing the offshore conditions driving extreme TWL_N. It is most likely, however, that the largest variability in local significant wave height is driven by the ebb tidal delta just offshore of the Golden Gate inlet [57]. This is evident in the alongshore variability of the wave conditions driving TWL_N compared to TWL_R. The offshore wave conditions driving extreme TWL_N at the southern edge of the delta are the most different from the offshore waves driving extreme TWL_R (Figures 5 and 6). Thus, similar to results from Hegermiller et al. [79], we find that the nearshore wave climate can be highly sensitive to changes in the deep-water wave climate, resulting in different controls on TWLs at each location.

Wave transformation and spatially-variable beach slope impact TWLs in slightly contrasting ways; wave transformation results in an overall decrease in TWL magnitude at all study sites while the local variation of the beach slope increases the magnitude of extreme TWLs when compared to TWL_R. Because the wave runup in this study is parameterized as a linear function of beach slope, the range and variance of TWLs increases across all locations when incorporating spatially-varying beach slopes in TWL computations. CA, which has lower waves and still water levels than both OR and WA, has the largest range of TWLs due to beach slope variability (Figure 7). Results exploring the influence of the temporal variability of beach slope on extreme TWLs are similar, where steeper profiles are more variable, resulting in a larger spread of extreme TWLs during the year at a specific profile.

The increase in the magnitude of TWLs due to the inclusion of beach slope variability also modifies how often a stretch of coastline is impacted by extreme TWLs. While wave transformation across the shelf influences which wave conditions generate extreme TWLs, the beach slope drives which locations may experience impacts from extreme TWL events. For example, extreme TWL_N usually impacted 100% or 0% of the coastline at once, and very few extreme TWL_N partially impacted the coastline. However, there was an increase in partial collision when the collision regime was computed using extreme $TWL_{N\beta_Y}$. This displays that impact hours per year are more dependent on spatial variations in beach morphology rather than spatial variations in the wave climate. These results are backed by shoreline change estimates at each site; OR, which has had the most long-term erosion, is estimated to experience the most impacts of all sites, while WA, which has been generally prograding, is estimated to experience the least amount of impacts.

The relationship between the standard deviation of the temporally-varying beach slope and the average beach slope shows that the average beach slope may provide a reasonable estimate of TWLs at a specific location for shallow-sloping, less variable beach profiles. However, the spatial variability of beach slope on flat beaches may incompletely represent the influence of the temporal variability in beach slope on extreme TWLs. Thus, characterizing the temporal variability in beach slope may be more important to consider at locations where hotspot erosion persists rather than on an already spatially variable coastline. These results may have implications for understanding the necessary spatial and temporal resolutions for survey design in long term coastal monitoring programs.

4.1. Defining Extreme Total Water Level Events

An extreme event is traditionally defined as an occurrence of a value over (or under) some threshold near the upper (or lower) ends of the range of observed values [80]. Here, our research suggests that the largest TWL events in any given year along the Washington, Oregon, and California coastlines are not always driven by extraordinarily large wave events. Similar to Serafin et al. [27], results indicate that the 10 largest TWL events every year can occur even when wave heights are less than the annual wave average during high tides.

Moreover, calculation of TWLs using the offshore wave climate may not explain all of the conditions driving extreme TWLs at a specific site. Erikson et al. [47] have described similar results on the southern California coast; low probability events, such as the 100-yr return level event, are usually forced by the same storm over an entire region. However, wave transformation processes and local variation in water levels define the local drivers of extreme events during higher probability extreme events (e.g., the annual event or the 20-yr return level event). Therefore, when considering extreme event scenarios, depending on the magnitude and frequency of the event, it is important to consider locally derived estimates of more frequent extremes, rather than only regional estimates based on offshore, spatially-uniform forcing.

How then should extreme water level events be defined? The locations with the largest magnitude TWLs do not always coincide with the highest impacts. Thus, evaluating only the magnitude of events does little to describe local conditions relative to shaping coastlines. Risk-based approaches focus on conditions driving a response variable (e.g., extent flooded, storm-induced erosion, impact hours per year) rather than a description based on a 'design' event [81]. The average differences between the magnitude of TWL_R, TWL_N, and $TWL_{N\beta_Y}$ at all three sites is small, often less than 50 cm. Impacts, however, are often defined by meeting or exceeding some threshold, and once that threshold is met, the consequences can be large. Here, seemingly small changes in TWLs (e.g., less than 10%) are shown to drive large changes in impact hours per year, pointing to the threshold nature of extreme water level events in coastal settings. Based on this assessment, it is important to consider a full distribution of forcings in order to adequately define which events may result in extreme impacts to an area.

4.2. Linking Hypothetical Future Wave Climates to Local Coastal Hazards

Although wave-induced water levels are a major component of extreme erosion events, changes to the wave climate and/or beach morphology are rarely considered when projecting future coastal hazards. Thus, hypothetical future climate scenarios developed around a range of recent projections provide an estimate of how shifts to the deep-water wave climate may alter local coastal hazards. Results indicate that the same shifts to the future wave climate, beach morphology, and sea level, drive location-dependent differences in the magnitude of TWLs and their resulting impacts.

Our research approximates coastal change through proxies, however, coastal change is often a function of both cross-shore and longshore sediment transport gradients. While changes to wave direction are known to result in spatial changes (erosion and accretion) of sandy coastlines due to deviations in longshore sediment transport [82], the influence of wave direction on the elevation of total water levels is often overlooked. Recently, Harley et al. [83] measured the largest-magnitude of an Australian beach's volume change in four decades from an extratropical storm with an anomalous wave direction. Our analysis shows, that in certain locations, changes to the wave direction may alter TWLs just as much as changes in wave height. For example, in CA, a 5% anticlockwise (more waves arriving from the south) rotation of the wave climate (approximately 5°) impacts coastlines as much as a 5% increase in the wave height (approximately 13 cm).

Increases or decreases to the average wave height, which often is the focus of many studies investigating the potential for future changes in storminess, drives some of the lowest overall changes in extreme TWLs at all locations. The largest changes at all sites are produced instead by a change in peak wave period. While it may be more likely for wave height to change by 10% than a 10% change in peak wave period, an increase in peak wave period by as little as 2% would increase impacts by 10 to 15%. This is similar to the impacts from a 5-10% increase in wave height at CA, and a 10-15% in wave height at WA and OR. While wave transformation processes have the smallest effect on TWLs in WA, WA is the most impacted by changes in peak period. This is due to the addition of increased $R_{2\%}$ on high still water levels. Across all locations, OR is the least affected by changes to the overall wave climate, likely because it is already in a predominantly erosional state.

Sea level has risen and is projected to continue rising [84, 10, 75], putting many coastal communities at risk of nuisance [11, 85, 86] and catastrophic flooding and erosion events. Not surprisingly, changes to mean sea level increase impact hours per year across all locations. However, the same increase in sea level has a very different effect on each location. Because sea level is the largest contributor to TWLs in WA, its impact is largest in WA, followed by OR, and CA.

Finally, our analysis investigates how specific coastal adaptation strategies could alter future coastal impacts. By allowing for steepening and flattening of beach slopes by 1/100 the impact nourishment or armoring projects could have on the coast is assessed. OR and CA, which represent the steepest beaches, would see the largest reduction in IHPY (by up to 50%) from a flattening of beach profile. For all cases, impacts due to morphological change are larger than future changes to wave height and direction. Thus, future research should focus on assessing both the uncertainties that exist in projecting future coastal hazards on present-day morphology, as well as the role human interventions may have on future coastal hazards.

4.3. Assumptions

Our research explores the role that future changes to the wave climate may have on the magnitude and impacts of extreme coastal TWLs. This study applies the widely used Stockdon et al. [23] formulation as it has been shown to have meaningful predictive skill [21, 19, 22] and has been the basis of operational predictions of morphological change in the United States for nearly a decade [73]. There are many other formulations available for sandy beaches [87, 88, 89] as well as other formulations suited for environments other than sandy beaches, like gravel [18] or engineered coastlines [90]. Testing alternative sandy beach formulations (not shown) produced modest variations in the magnitude of wave runup, however, it did not alter the overall trends and conclusions of our results. Nevertheless, any empirical parameterization based on field or laboratory data is limited by the conditions captured during experiments. While the use of numerical models has become more prevalent in understanding extreme runup events (e.g., [21]), these models are typically too computationally expensive to run across large stretches of the coastline. Ultimately, more research is needed on understanding wave runup in extreme conditions.

While this research recognizes the influence that spatially and temporally variable beach slopes have on TWLs, the alongshore variability of beach slope is smoothed along the coastline into 100 m bins and the average beach slope in that 100 m stretch of coast is used for TWL computations. In order to perform a detailed, site-specific assessment of impacts of extreme TWLs, it would be important to understand the distribution of beach slopes within each spatial bin to incorporate a full range of uncertainty related to beach slope in TWL elevations. One example technique in doing so is already implemented in the U.S. Geological Survey [33] storm impact assessments (https://marine.usgs.gov/coastalchangehazardsportal/) where beach slope variability is included as a measure of uncertainty within TWL computations, allowing for both hydrodynamic and morphologic influences within their probabilistic coastal hazard assessments. We futher simplify the morphological variability at each study site by calculating the collision regime and impact hours per year over a single contour representing the dune toe. Alongshore-varying dune erosion during storms has been found to be linked to the pre-storm elevation of the dune toe with respect to the TWL [91], thus removing the spatial variability of the dune contour may alter the variability of impacts. While further investigation of the controls on coastal impacts will continue to link TWL magnitudes to local-scales, this simplification was necessary to disentangle the other relative morphological controls on TWLs.

Our analysis investigates future changes to the average distribution of each wave climate variable while assuming each variable will change independently of one another. It is, however, more likely that changes to the wave environment will occur concurrently due to the dependencies between wave height, period, and direction, driving nonlinearities in coastal TWLs. For example, Erikson et al. [42] project a decrease in the mean significant wave height of 50 cm (approximately 17% of present day) and an increase in the mean wave period by approximately 0.5 s (approximately 5% of present day), likely due to a shift in storm tracks towards the north along the US West coast. Combined, an increase in wave period and a simultaneous decrease in wave height may have contrasting effects on a location's impact hours per year. It is also more likely average and extreme conditions may be modified by the future global climate in different ways. For example, Wang et al. [39] show that while the annual average wave height may decrease across the US West coast, annual maximum and winter wave heights may increase. Future research will further investigate both the concurrent impacts of altering wave climate variables together as well as handling extreme conditions differently than average conditions.

Our research highlights the complexities that exist in understanding the controls on local coastal hazards. While the influence of morphological variables on coastal water levels is often overlooked in predictions of future coastal hazards, there are many other variables that could change, thus altering the magnitude of nearshore TWLs. Rising sea levels slowly increases the baseline of the mean sea level, which in turn increases the frequency of nuisance [86, 92, 85, 11] and catastrophic flooding events. This work simplifies the relationship between wave-driven water levels and coastal impacts and does not consider the nonlinear amplifications of waves on top of storm surge [93], nonlinear interactions between storm surge and sea level rise [94, 95] changes to tidal hydrodynamics [96, 97], or variation in storm surge due to changes in storminess. Each of these aforementioned variations to the components of TWLs will also play a role in future changes to TWLs.

5. Conclusions

Regional variations in total water levels (TWLs) are influenced by a combination of oceanographic and geomorphological processes. Differences in shelf bathymetry, coastal orientation, beach slope, wave climate, storm surge, tidal range, seasonality, and interannual water levels drive variation in locally-generated extreme TWLs and their resulting impacts. While our results are specific to three sites along the US West coast, we find some general conclusions important to many sandy beaches around the globe.

First, extreme TWLs are generated by a distribution of forcings, including waves less than the average annual wave height. Thus, seemingly small storm events paired with high still water levels could be responsible for some of the largest TWLs in any given year. Next, beach topography and shelf bathymetry both play an important role in influencing the magnitude of TWLs and their corresponding impacts. While the specific storm events affecting the coastline are explained by wave transformation over the shelf, the spatially-variable impacts of extreme TWLs (e.g., how much the coastline is impacted at once by a storm event) are driven by the spatially-varying beach slope. Steeper beach slopes drive higher TWLs, and a large range in the spatial variability of beach slope likely characterizes the temporal variability of beach slope along relatively steeper stretches of coastline. On the other hand, the variance of the spatial variability of beach slope along overall flat stretches of coastline may not characterize the true range of temporally-varying beach slope and underestimate TWLs.

Because wave transformation across the shelf determines which storm events affect the coastline, the same deep-water change to the wave climate could result in different impacts at regionally close locations. Regardless of the large-scale change to the wave climate, wave transformation processes could amplify or suppress the magnitude of local TWLs, depending on the relative contribution of the TWL as well as the complexity of the local shelf. The consideration of changes to the wave climate is thus important for understanding local-scale hazards. For example, a change in wave direction may increase the impacts of TWLs as much as a change in wave height. Furthermore, changes to the wave period drive the largest increase in TWLs and their resulting impacts, suggesting that future projections of this variable should be more heavily researched. Finally, risk-based approaches defining extreme water level events based on impacts rather than design events are necessary for reducing the exposure of communities to coastal hazards, as small changes in TWLs can drive large, nonlinear changes in impacts. Overall, this research provides some first steps for highlighting the complexities that exist when considering the impact of future TWLs along coastlines.

6. Acknowledgements

Tide gauge records are available through the National Oceanic and Atmospheric Administration (NOAA) National Ocean Service (NOS) website. We thank Melisa Menéndez and Jorge Pérez at the Environmental Hydraulics Institute of the Universidad de Catanbria (IHCantabria) for providing the Global Ocean Wave 2 (GOW2) data. Thank you to all the individuals at the Washington Department of Ecology, U.S. Geological Survey (USGS), and Oregon State University who participated in the collection of the beach profile data, as well as the Northwest Association of Networked Ocean Observing System (NANOOS) for supporting some of the observations. Thank you also to Daniel Hoover who provided topographic surveys of Ocean Beach in the San Francisco Littoral Cell, Tuba Özkan-Haller who provided comments on an early draft, Davina Passeri who provided the USGS internal review, and Robert Hatfield who assisted in figure editing. Comments from two anonymous reviewers significantly improved the clarity of this manuscript.

This work was funded by the USGS, the NOAA Regional Integrated Sciences and Assessments (RISA) program (NA10OAR4310218 and NA15OAR4310145), NOAA's Coastal and Ocean Climate Applications (COCA) program (NA15OAR4310243), and the Geomorphology and Land Use Dynamics program at the National Science Foundation (award EAR-1531512).

Appendix A. Hydrodynamic Datasets

The primary tide gauge for the North Beach subcell (WA) is Westport (NOAA station 941102) which was merged with Toke Point (NOAA station 9440910) located 20 km south. Before combining records, both tide gauges were decomposed into low and high frequency water level signals (e.g. seasonality, η_{SE}; monthly mean sea level anomalies, η_{MMSLA}; and storm surge, η_{SS}, respectively; see supporting information from [27] for a description of the decomposition methods). Water level components affected by regional or local forcings driving site-specific variations in η_{MMSLA} and η_{SS} were compared between the primary and secondary tide gauge records before combining. Components deterministic to the primary tide gauge (i.e., tides and seasonality; η_A and η_{SE}) were extended over the whole record length for the combined record.

η_{MMSLA} between Westport and Toke Point tide gauges were similar, with an $R^2 = 0.96$ and an overall bias of less than 1 cm. The η_{MMSLA} were therefore combined by merging with no further alteration: Toke Point η_{MMSLA} were added to the beginning of the Westport η_{MMSLA} record. Toke Point, however, has higher magnitude η_{SS} than other stations in the region and although the Westport and Toke Point stations were well correlated ($R^2 = 0.94$), there was a noticeable offset when comparing the most extreme storm surge peaks (black dots, Figure Appendix A.1). When the η_{SS} at the Westport tide gauge was greater than 0.5 m, the η_{SS} at Toke Point was on average 15 cm larger, with a maximum offset of 60 cm. In order to correct for this offset between the extreme η_{SS} signals at each station, a linear model was fit to the relationship between the two tide gauge records (blue line, Figure Appendix A.1).

Toke Point η_{SS} was allocated into 1 cm bins from -0.8 to 1.5 m and the difference between the linear model fit to the joint relationship between the Westport and Toke Point tide gauge and a 1-to-1 model between the two tide gauges was computed for each bin (blue line and green line in Figure Appendix A.1, respectively). This "correction" (the difference between the linear model and the 1-to-1 model at each bin) was then subtracted from the Toke Point η_{SS} time series to decrease the magnitude of the signal, bringing it closer to the values of the

η_{SS} at the Westport tide gauge (red dots, Figure Appendix A.1). Each of the decomposed signals (i.e., η_A, η_{MSL}, η_{SE}, η_{SS}, η_{MMSLA}) were then added together to create a "combined" still water level record with a record length of at least 30 years at the primary tide gauge location.

A combined record was also necessary at the Netarts Littoral Cell (OR) study site. The Garibaldi tide gauge (NOAA station 9437540), is located in Tillamook Bay, 10 km north of Garibaldi Bay, making it the closest tide gauge record and thus the primary tide gauge for the OR. It was merged with the South Beach (NOAA station 9435380) tide gauge located 90 km south in Yaquina Bay near Newport, OR. Storm surges were well matched between the two tide gauges, so no linear correction, like what was used for the WA study site, was necessary. As in WA, components deterministic to the primary tide gauge (i.e., η_A and η_{SE}) were used over the whole record length. Each decomposed signal was merged between tide gauges by combining signals from the start date of the secondary tide gauge to the beginning of the primary tide gauge. The San Francisco tide gauge (NOAA station 9414290) was sufficiently long, so no tide gauge merging was necessary for the San Francisco Littoral Cell (CA) study site.

Appendix B. Morphologic Datasets

In order to evaluate how the alongshore variation in beach topography affects TWLs, lidar from a 2002 NASA/USGS survey (for Washington and Oregon; [69]) and lidar from a 1998 NOAA/NASA/USGS survey (for California; [70]) were interpolated to evenly spaced grids and morphometrics such as dune/bluff/structure crest, dune/bluff/structure toe, shoreline, and backshore beach slope were selected every 5-10 m in Oregon and Washington [68] and at a slightly courser resolution for California [65]. The shoreline was extracted from lidar data using the operational mean high water (MHW) elevation, which represents an average of MHW elevations from individual open-ocean or near-open-ocean tide gauges [98]. The operational MHW elevation is 2.1 m NAVD88 in NBSC and NLC and 1.46 m NAVD88 in SFLC. The backshore beach slope (β) was computed as the best fit line between the dune/bluff/structure toe and the datum-based shoreline. This provides a spatially-varying,

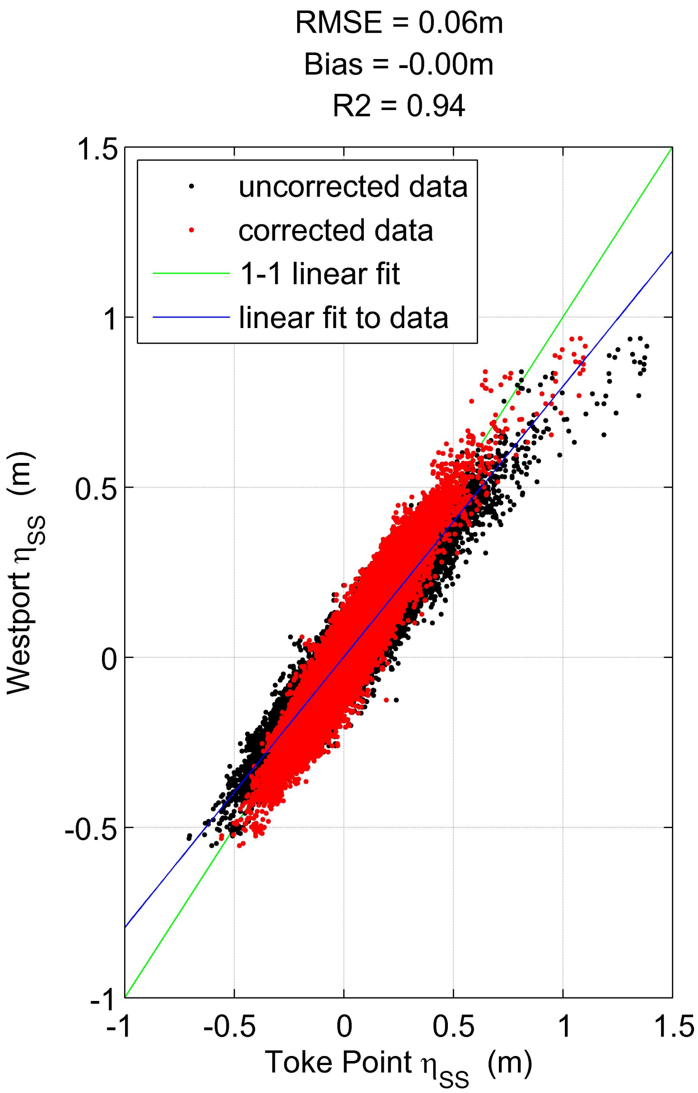

Figure Appendix A.1: Comparison of storm surge (η_{SS}) from the primary Westport tide gauge and the secondary Toke Point tide gauge for the North Beach Subcell, WA study site. Black dots indicate the original η_{SS} signal, while red dots indicate the η_{SS} post-correction. The blue line represents a linear fit between the Westport and Toke Point η_{SS}, while the green line represents a 1-to-1 line.

Table Appendix B.1: Data availability of topographic beach surveys at each study site used for extracting temporally-varying beach slopes for extreme TWL computations.

Location	Dates	Time	Number of surveys
North Beach Subcell, WA	1997 - 2015	quarterly	72
Netarts Littoral Cell, OR	2015 - 2016	monthly	12
San Francisco Littoral Cell, CA	2004 - 2015	monthly	147

consistently-defined beach slope across all three locations. Estimates of beach slope were averaged over 100 m bin spacing to avoid abrupt transitions, but statistics such as the standard deviation, maximum, and minimum across each 100 m bin were retained for further analysis.

Real-Time Kinematic- Differential Global Positioning System (RTK-DGPS) equipment mounted on a backpack or ATV was used to survey profiles across the beach face to the foredune or to the base of coastal bluffs or shore protection structures. Profile measurements in NBSC were surveyed on a quarterly basis from 1997 - present as part of a larger field monitoring program of the entire CRLC [58, 99], while measurements at SFLC were surveyed monthly to characterize long-term, seasonal, and storm-induced variability of the system from 2004 - present [55]. The NLC was surveyed monthly during the 2015/16 El Niño season (Table Appendix B.1).Estimates of beach slope (whether spatially or temporally varying) were capped at 1/8, the limit to beach slopes used during the field measurements for the selected runup parameterization [100].

References

[1] I. D. Haigh, M. Eliot, C. Pattiaratchi, Global influences of the 18.61 year nodal cycle and 8.85 year cycle of lunar perigee on high tidal levels, Journal of Geophysical Research: Oceans 116 (C6).

[2] T. Wahl, F. M. Calafat, M. E. Luther, Rapid changes in the seasonal sea level cycle along the US Gulf coast from the late 20th century, Geophysical Research Letters 41 (2) (2014) 491–498.

[3] M. A. Merrifield, A. S. Genz, C. P. Kontoes, J. J. Marra, Annual maximum water levels from tide gauges: Contributing factors and geographic patterns, Journal of Geophysical Research: Oceans 118 (5) (2013) 2535–2546.

[4] M. Tsimplis, P. Woodworth, The global distribution of the seasonal sea level cycle calculated from coastal tide gauge data, Journal of Geophysical Research: Oceans 99 (C8) (1994) 16031–16039.

[5] D. B. Chelton, D. B. Enfield, Ocean signals in tide gauge records, Journal of Geophysical Research: Solid Earth 91 (B9) (1986) 9081–9098.

[6] P. D. Komar, J. C. Allan, P. Ruggiero, Sea level variations along the US Pacific Northwest coast: Tectonic and climate controls, Journal of Coastal Research 27 (5) (2011) 808–823.

[7] R. E. Kopp, J. X. Mitrovica, S. M. Griffies, J. Yin, C. C. Hay, R. J. Stouffer, The impact of Greenland melt on local sea levels: a partially coupled analysis of dynamic and static equilibrium effects in idealized water-hosing experiments, Climatic Change 103 (3-4) (2010) 619–625.

[8] J. A. Church, N. J. White, Sea-level rise from the late 19th to the early 21st century, Surveys in Geophysics 32 (4-5) (2011) 585–602.

[9] R. Nerem, D. Chambers, C. Choe, G. Mitchum, Estimating mean sea level change from the TOPEX and Jason altimeter missions, Marine Geodesy 33 (S1) (2010) 435–446.

[10] R. Nerem, B. Beckley, J. Fasullo, B. Hamlington, D. Masters, G. Mitchum, Climate-change–driven accelerated sea-level rise detected in the altimeter era, Proceedings of the National Academy of Sciences (2018) 201717312.

[11] S. Vitousek, P. L. Barnard, C. H. Fletcher, N. Frazer, L. Erikson, C. D. Storlazzi, Doubling of coastal flooding frequency within decades due to sea-level rise, Scientific Reports 7 (1) (2017) 1399.

[12] W. V. Sweet, Sea level rise and nuisance flood frequency changes around the United States, US Department of Commerce, National Oceanic and Atmospheric Administration, National Ocean Service, Center for Operational Oceanographic Products and Services, 2014.

[13] P. Ruggiero, R. A. Holman, R. Beach, Wave run-up on a high-energy dissipative beach, Journal of Geophysical Research: Oceans (1978–2012) 109 (C6).

[14] B. Ruessink, M. Kleinhans, P. den Beukel, Observations of swash under highly dissipative conditions, Journal of Geophysical Research: Oceans 103 (C2) (1998) 3111–3118.

[15] R. A. Holman, A. Sallenger, Setup and swash on a natural beach, Journal of Geophysical Research: Oceans (1978–2012) 90 (C1) (1985) 945–953.

[16] M. S. Longuet-Higgins, R. Stewart, Radiation stresses in water waves; a physical discussion, with applications, in: Deep Sea Research and Oceanographic Abstracts, Elsevier, 1964, pp. 529–562.

[17] J. W. Fiedler, P. B. Smit, K. L. Brodie, J. McNinch, R. Guza, Numerical modeling of wave runup on steep and mildly sloping natural beaches, Coastal Engineering 131 (2018) 106–113.

[18] T. G. Poate, R. T. McCall, G. Masselink, A new parameterisation for runup on gravel beaches, Coastal Engineering 117 (2016) 176–190.

[19] N. Cohn, P. Ruggiero, The influence of seasonal to interannual nearshore profile variability on extreme

water levels: Modeling wave runup on dissipative beaches, Coastal Engineering 115 (2016) 79–92.

[20] J. W. Fiedler, K. L. Brodie, J. E. McNinch, R. T. Guza, Observations of runup and energy flux on a low-slope beach with high-energy, long-period ocean swell, Geophysical Research Letters 42 (22) (2015) 9933–9941.

[21] H. F. Stockdon, D. M. Thompson, N. G. Plant, J. W. Long, Evaluation of wave runup predictions from numerical and parametric models, Coastal Engineering 92 (2014) 1–11.

[22] N. Senechal, G. Coco, K. R. Bryan, R. A. Holman, Wave runup during extreme storm conditions, Journal of Geophysical Research: Oceans 116 (C7).

[23] H. F. Stockdon, R. A. Holman, P. A. Howd, A. H. Sallenger Jr, Empirical parameterization of setup, swash, and runup, Coastal Engineering 53 (7) (2006) 573–588.

[24] J. De Waal, J. Van der Meer, Wave runup and overtopping on coastal structures, in: Coastal Engineering 1992, 1993, pp. 1758–1771.

[25] P. Ruggiero, P. D. Komar, W. G. McDougal, J. J. Marra, R. A. Beach, Wave runup, extreme water levels and the erosion of properties backing beaches, Journal of Coastal Research (2001) 407–419.

[26] A. Melet, B. Meyssignac, R. Almar, G. Le Cozannet, Under-estimated wave contribution to coastal sea-level rise, Nature Climate Change 8 (3) (2018) 234.

[27] K. A. Serafin, P. Ruggiero, H. F. Stockdon, The relative contribution of waves, tides, and nontidal residuals to extreme total water levels on US West coast sandy beaches, Geophysical Research Letters 44 (4) (2017) 1839–1847.

[28] A. Melet, R. Almar, B. Meyssignac, What dominates sea level at the coast: a case study for the Gulf of Guinea, Ocean Dynamics (2016) 1–14.

[29] M. I. Vousdoukas, Developments in large-scale coastal flood hazard mapping, Natural Hazards and Earth System Sciences 16 (8) (2016) 1841.

[30] K. A. Serafin, P. Ruggiero, Simulating extreme total water levels using a time-dependent, extreme value approach, Journal of Geophysical Research: Oceans 119 (9) (2014) 6305–6329.

[31] P. Ruggiero, Is the intensifying wave climate of the US Pacific Northwest increasing flooding and erosion risk faster than sea-level rise?, Journal of Waterway, Port, Coastal, and Ocean Engineering 139 (2) (2013) 88–97.

[32] L. Wright, A. D. Short, Morphodynamic variability of surf zones and beaches: A synthesis, Marine Geology 56 (1-4) (1984) 93–118.

[33] K. S. Doran, J. W. Long, J. R. Overbeck, A method for determining average beach slope and beach slope variability for US sandy coastlines, Tech. rep., US Geological Survey (2015).

[34] K. L. Brodie, R. K. Slocum, J. E. McNinch, New insights into the physical drivers of wave runup from a continuously operating terrestrial laser scanner, in: Oceans, 2012, IEEE, 2012, pp. 1–8.

[35] N. Senechal, G. Coco, K. Bryan, J. MacMahan, J. Brown, R. Holman, Tidal effects on runup in presence of complex 3D morphologies under dissipative surf zone conditions, in: Coastal Dynamics, Vol. 2013, 2013, pp. 1483–1494.

[36] G. García-Medina, H. T. Özkan-Haller, P. Ruggiero, J. Oskamp, An inner-shelf wave forecasting system for the US Pacific Northwest, Weather and Forecasting 28 (3) (2013) 681–703.

[37] W. C. O'Reilly, The southern California wave climate: effects of islands and bathymetry, Shore & Beach 61 (3) (1993) 14–19.

[38] W. H. Munk, M. A. Traylor, Refraction of ocean waves: a process linking underwater topography to beach erosion, The Journal of Geology 55 (1) (1947) 1–26.

[39] X. L. Wang, Y. Feng, V. R. Swail, Changes in global ocean wave heights as projected using multimodel CMIP5 simulations, Geophysical Research Letters 41 (3) (2014) 1026–1034.

[40] M. A. Hemer, Y. Fan, N. Mori, A. Semedo, X. L. Wang, Projected changes in wave climate from a multi-model ensemble, Nature Climate Change 3 (5) (2013) 471–476.

[41] T. Shimura, N. Mori, M. A. Hemer, Variability and future decreases in winter wave heights in the Western North Pacific, Geophysical Research Letters 43 (6) (2016) 2716–2722.

[42] L. Erikson, C. Hegermiller, P. Barnard, P. Ruggiero, M. van Ormondt, Projected wave conditions in the Eastern North Pacific under the influence of two CMIP5 climate scenarios, Ocean Modelling 96 (2015) 171–185.

[43] M. Casas-Prat, J. Sierra, Projected future wave climate in the NW Mediterranean Sea, Journal of Geophysical Research: Oceans 118 (7) (2013) 3548–3568.

[44] E. Charles, D. Idier, P. Delecluse, M. Déqué, G. Le Cozannet, Climate change impact on waves in the Bay of Biscay, France, Ocean Dynamics 62 (6) (2012) 831–848.

[45] W. Cai, S. Borlace, M. Lengaigne, P. Van Rensch, M. Collins, G. Vecchi, A. Timmermann, A. Santoso, M. J. McPhaden, L. Wu, et al., Increasing frequency of extreme El Niño events due to greenhouse warming, Nature Climate Change 4 (2) (2014) 111–116.

[46] J. B. Shope, C. D. Storlazzi, R. K. Hoeke, Projected atoll shoreline and run-up changes in response to sea-level rise and varying large wave conditions at Wake and Midway Atolls, Northwestern Hawaiian islands, Geomorphology 295 (2017) 537–550.

[47] L. H. Erikson, A. Espejo, P. L. Barnard, K. A. Serafin, C. A. Hegermiller, A. O'Neill, P. Ruggiero, P. W. Limber, F. J. Mendez, Identification of storm events and contiguous coastal sections for deterministic modeling of extreme coastal flood events in response to climate change, Coastal Engineering 140 (2018) 316–330.

[48] P. L. Barnard, M. van Ormondt, L. H. Erikson, J. Eshleman, C. Hapke, P. Ruggiero, P. N. Adams, A. C. Foxgrover, Development of the Coastal Storm Modeling System (CoSMoS) for predicting the

impact of storms on high-energy, active-margin coasts, Natural Hazards 74 (2) (2014) 1095–1125.

[49] J. Sierra, M. Casas-Prat, Analysis of potential impacts on coastal areas due to changes in wave conditions, Climatic change 124 (4) (2014) 861–876.

[50] J. B. Shope, C. D. Storlazzi, L. H. Erikson, C. A. Hegermiller, Changes to extreme wave climates of islands within the Western Tropical Pacific throughout the 21st century under RCP 4.5 and RCP 8.5, with implications for island vulnerability and sustainability, Global and Planetary Change 141 (2016) 25–38.

[51] A. K. Mills, J. P. Bolte, P. Ruggiero, K. A. Serafin, E. Lipiec, P. Corcoran, J. Stevenson, C. Zanocco, D. Lach, Exploring the impacts of climate and policy changes on coastal community resilience: Simulating alternative future scenarios, Environmental Modelling & Software 109 (2018) 80–92.

[52] R.-Q. Wang, M. T. Stacey, L. Herdman, P. Barnard, L. Erikson, The influence of sea level rise on the regional interdependence of coastal infrastructure, Earth's Future.

[53] R.-Q. Wang, L. M. Herdman, L. Erikson, P. Barnard, M. Hummel, M. T. Stacey, Interactions of estuarine shoreline infrastructure with multiscale sea level variability, Journal of Geophysical Research: Oceans 122 (12) (2017) 9962–9979.

[54] P. Ruggiero, G. M. Kaminsky, G. Gelfenbaum, N. Cohn, Morphodynamics of prograding beaches: A synthesis of seasonal-to century-scale observations of the Columbia River Littoral Cell, Marine Geology 376 (2016) 51–68.

[55] J. E. Hansen, P. L. Barnard, Sub-weekly to interannual variability of a high-energy shoreline, Coastal Engineering 57 (11) (2010) 959–972.

[56] P. L. Barnard, J. E. Hansen, L. H. Erikson, Synthesis study of an erosion hot spot; Ocean Beach, California, Journal of Coastal Research 28 (4) (2012) 903–922.

[57] J. L. Eshleman, P. L. Barnard, L. H. Erikson, D. M. Hanes, Coupling alongshore variations in wave energy to beach morphologic change using the SWAN wave model at Ocean Beach, San Francisco, CA, in: 10th International Workshop on Wave Hindcasting and Forecasting (Oahu, Hawaii), Paper F, Vol. 4, 2007, p. 20p.

[58] P. Ruggiero, G. M. Kaminsky, G. Gelfenbaum, B. Voigt, Seasonal to interannual morphodynamics along a high-energy dissipative littoral cell, Journal of Coastal Research (2005) 553–578.

[59] D. Di Leonardo, P. Ruggiero, Regional scale sandbar variability: Observations from the US Pacific Northwest, Continental Shelf Research 95 (2015) 74–88.

[60] NOAA, Tides & Currents, Center of Operational Products and Services, http://tidesandcurrents.noaa.gov.

[61] J. Allan, P. Ruggiero, G. Garcia-Medina, F. O'Brien, S. LL, J. Roberts, Coastal flood hazard study, Tillamook County, Oregon: Oregon Department of Geology and Mineral Industries special paper 47,

274p (2015).

[62] P. Komar, J. Good, S. Shih, Erosion of Netarts Spit, Oregon: Continued impacts of the 1982-83 El Niño, Shore and Beach 57 (1) (1989) 11–19.

[63] D. L. Revell, P. D. Komar, A. H. Sallenger Jr, An application of lidar to analyses of El Niño erosion in the Netarts Littoral Cell, Oregon, Journal of Coastal Research (2002) 792–801.

[64] K. L. Dallas, P. L. Barnard, Anthropogenic influences on shoreline and nearshore evolution in the San Francisco Bay coastal system, Estuarine, Coastal and Shelf Science 92 (1) (2011) 195–204.

[65] C. J. Hapke, D. Reid, B. M. Richmond, P. Ruggiero, J. List, National assessment of shoreline change part 3: Historical shoreline change and associated coastal land loss along sandy shorelines of the California coast, US Geological Survey Open File Report 1219 (2006) 79.

[66] P. L. Barnard, J. Eshleman, L. H. Erikson, D. M. Hanes, Coastal processes study at Ocean Beach, San Francisco, CA: summary of data collection 2004-2006, Tech. rep., US Geological Survey (2007).

[67] J. Pérez, M. Menéndez, I. J. Losada, GOW2: A global wave hindcast for coastal applications, Coastal Engineering 124 (2017) 1–11.

[68] J. Mull, P. Ruggiero, Estimating storm-induced dune erosion and overtopping along US West coast beaches, Journal of Coastal Research 30 (6) (2014) 1173–1187.

[69] OCM, 2002 NASA/USGS Airborne lidar assessment of coastal erosion (ALACE) project for California, Oregon, and Washington coastline, https://inport.nmfs.noaa.gov/inport/item/4963.

[70] OCM, 1998 Spring west coast (post El Nino) NOAA/NASA/USGS Airborne lidar assessment of coastal erosion (ALACE) project for the US coastline, https://inport.nmfs.noaa.gov/inport/item/48155.

[71] N. Booij, R. Ris, L. H. Holthuijsen, A third-generation wave model for coastal regions: 1. model description and validation, Journal of Geophysical Research: Oceans (1978–2012) 104 (C4) (1999) 7649–7666.

[72] R. L. Smith, Extreme value theory based on the r–largest annual events, Journal of Hydrology 86 (1-2) (1986) 27–43.

[73] H. F. Stockdon, A. H. Sallenger, R. A. Holman, P. A. Howd, A simple model for the spatially-variable coastal response to hurricanes, Marine Geology 238 (1) (2007) 1–20.

[74] A. H. Sallenger, Storm impact scale for barrier islands, Journal of Coastal Research (2000) 890–895.

[75] W. V. Sweet, R. E. Kopp, C. P. Weaver, J. Obeysekera, R. M. Horton, E. R. Thieler, C. Zervas, Global and regional sea level rise scenarios for the United States.

[76] R. E. Kopp, R. M. Horton, C. M. Little, J. X. Mitrovica, M. Oppenheimer, D. Rasmussen, B. H. Strauss, C. Tebaldi, Probabilistic 21st and 22nd century sea-level projections at a global network of tide-gauge sites, Earth's Future 2 (8) (2014) 383–406.

[77] T. Wahl, N. G. Plant, Changes in erosion and flooding risk due to long-term and cyclic oceanographic

trends, Geophysical Research Letters 42 (8) (2015) 2943–2950.

[78] C. D. Storlazzi, D. K. Wingfield, Spatial and temporal variations in oceanographic and meteorologic forcing along the central california coast, 1980-2002, Tech. rep. (2005).

[79] C. A. Hegermiller, A. Rueda, L. H. Erikson, P. L. Barnard, J. A. Antolinez, F. J. Mendez, Controls of multimodal wave conditions in a complex coastal setting, Geophysical Research Letters 44 (24).

[80] M. Leonard, S. Westra, A. Phatak, M. Lambert, B. van den Hurk, K. McInnes, J. Risbey, S. Schuster, D. Jakob, M. Stafford-Smith, A compound event framework for understanding extreme impacts, Wiley Interdisciplinary Reviews: Climate Change 5 (1) (2014) 113–128.

[81] B. Gouldby, D. Wyncoll, M. Panzeri, M. Franklin, T. Hunt, D. Hames, N. Tozer, P. Hawkes, U. Dornbusch, T. Pullen, Multivariate extreme value modelling of sea conditions around the coast of England, in: Proceedings of the Institution of Civil Engineers-Maritime Engineering, 2017, pp. 3–20.

[82] K. D. Splinter, M. A. Davidson, A. Golshani, R. Tomlinson, Climate controls on longshore sediment transport, Continental Shelf Research 48 (2012) 146–156.

[83] M. D. Harley, I. L. Turner, M. A. Kinsela, J. H. Middleton, P. J. Mumford, K. D. Splinter, M. S. Phillips, J. A. Simmons, D. J. Hanslow, A. D. Short, Extreme coastal erosion enhanced by anomalous extratropical storm wave direction, Scientific Reports 7.

[84] J. A. Church, P. U. Clark, A. Cazenave, J. M. Gregory, S. Jevrejeva, A. Levermann, M. Merrifield, G. Milne, R. Nerem, P. Nunn, et al., Sea level change, Tech. rep., PM Cambridge University Press (2013).

[85] W. V. Sweet, J. Park, From the extreme to the mean: Acceleration and tipping points of coastal inundation from sea level rise, Earth's Future 2 (12) (2014) 579–600.

[86] H. R. Moftakhari, A. AghaKouchak, B. F. Sanders, D. L. Feldman, W. Sweet, R. A. Matthew, A. Luke, Increased nuisance flooding along the coasts of the United States due to sea level rise: Past and future, Geophysical Research Letters 42 (22) (2015) 9846–9852.

[87] R. Holman, Extreme value statistics for wave run-up on a natural beach, Coastal Engineering 9 (6) (1986) 527–544.

[88] M. I. Vousdoukas, D. Wziatek, L. P. Almeida, Coastal vulnerability assessment based on video wave run-up observations at a mesotidal, steep-sloped beach, Ocean Dynamics 62 (1) (2012) 123–137.

[89] A. L. Atkinson, H. E. Power, T. Moura, T. Hammond, D. P. Callaghan, T. E. Baldock, Assessment of runup predictions by empirical models on non-truncated beaches on the south-east australian coast, Coastal Engineering 119 (2017) 15–31.

[90] J. W. van der Meer, C.-J. M. Stam, Wave runup on smooth and rock slopes of coastal structures, Journal of Waterway, Port, Coastal, and Ocean Engineering 118 (5) (1992) 534–550.

[91] K. D. Splinter, E. T. Kearney, I. L. Turner, Drivers of alongshore variable dune erosion during a storm

event: Observations and modelling, Coastal Engineering 131 (2018) 31–41.

[92] R. D. Ray, G. Foster, Future nuisance flooding at Boston caused by astronomical tides alone, Earth's Future 4 (12) (2016) 578–587.

[93] A. Arns, S. Dangendorf, J. Jensen, S. Talke, J. Bender, C. Pattiaratchi, Sea-level rise induced amplification of coastal protection design heights, Scientific Reports 7 (2017) 40171.

[94] M. V. Bilskie, S. Hagen, K. Alizad, S. Medeiros, D. Passeri, H. Needham, A. Cox, Dynamic simulation and numerical analysis of hurricane storm surge under sea level rise with geomorphologic changes along the northern Gulf of Mexico, Earth's Future 4 (5) (2016) 177–193.

[95] M. Bilskie, S. Hagen, S. Medeiros, D. Passeri, Dynamics of sea level rise and coastal flooding on a changing landscape, Geophysical Research Letters 41 (3) (2014) 927–934.

[96] A. T. Devlin, D. A. Jay, S. A. Talke, E. D. Zaron, J. Pan, H. Lin, Coupling of sea level and tidal range changes, with implications for future water levels, Scientific reports 7 (1) (2017) 17021.

[97] D. L. Passeri, S. C. Hagen, N. G. Plant, M. V. Bilskie, S. C. Medeiros, K. Alizad, Tidal hydrodynamics under future sea level rise and coastal morphology in the Northern Gulf of Mexico, Earth's Future 4 (5) (2016) 159–176.

[98] K. M. Weber, J. H. List, K. L. Morgan, An operational mean high water datum for determination of shoreline position from topographic lidar data, Tech. rep. (2005).

[99] A. W. Stevens, G. Gelfenbaum, P. Ruggiero, G. M. Kaminsky, Southwest Washington littoral drift restoration–beach and nearshore morphological monitoring, Tech. rep., US Geological Survey (2012).

[100] H. F. Stockdon, K. S. Doran, A. H. Sallenger Jr, Extraction of lidar-based dune-crest elevations for use in examining the vulnerability of beaches to inundation during hurricanes, Journal of Coastal Research (2009) 59–65.